ISSN 1070-3284, Russian Journal of Coordination Chemistry, 2020, Vol. 46, No. 3, pp. 193–213. © Pleiades Publishing, Ltd., 2020.
Russian Text © The Author(s), 2020, published in Koordinatsionnaya Khimiya, 2020, Vol. 46, No. 3, pp. 172–192.

Mononuclear Cobalt and Iron *o*-Quinone Complexes with Tetradentate N-Donor Bases: Structures and Properties

A. A. Starikova[a], *, M. G. Chegerev[a], and A. G. Starikov[a]

[a] *Institute of Physical and Organic Chemistry, Southern Federal University, Rostov-on-Don, Russia*

**e-mail: alstar@ipoc.sfedu.ru*

Received September 25, 2019; revised October 28, 2019; accepted October 31, 2019

Abstract—Published data on the electronic structures and magnetic behavior of the mononuclear cobalt and iron *o*-benzoquinone complexes with tetradentate nitrogen-containing bases are reviewed. The chosen objects are of significant interest due to their ability to manifest magnetic bistability, indicating wide prospects of the practical use of compounds of this class in molecular electronics and spintronics. The influence of structural features of the complexes on their magnetic properties is discussed on the basis of the quantum-chemical calculation results.

Keywords: iron, cobalt, *o*-benzoquinone, tetraazamacrocyclic ligands, magnetic properties, electronic structure

DOI: 10.1134/S1070328420030070

INTRODUCTION

In the recent years, transition metal complexes with redox-active ligands became objects of intensive studies [1–20]. Increased attention to these systems is caused by their ability to demonstrate the mechanisms of magnetic bistability (spin crossover (SCO)) [21–24], valence tautomerism (VT) [25–27], and others and, as a consequence, the possibility of their use as molecular magnets, molecular switches, and spin qubits [28–37]. The abundant structural motif of magnetically active compounds is presented by the cationic metal (M) complexes bearing one redox-active ligand (Ln) and tetradentate nitrogen-containing macrocyclic base (TAMn, n = 1–5) (Scheme 1). Thus constructed molecules can manifest spin transitions due to VT [38] or SCO [39, 40], depending on the nature of the tetraazamacrocycle and metal (iron or cobalt), and can demonstrate the catalytic activity and imitate catechol dioxygenase [41, 42]. The present review is devoted to the systematic analysis of the electronic structures and magnetic properties of the compounds of the indicated type. The first part of the review contains the experimental data, and the results of the quantum chemical studies of the earlier synthesized and new cobalt and iron o-benzoquinone complexes with tetraazamacrocyclic ligands are considered in the second part.

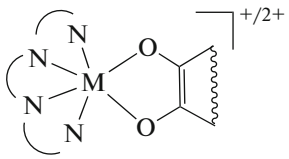

M = Co, Fe

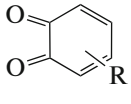

R = H (a),
3,5-*t*-Bu_2 (b),
3,4,5,6-Cl_4 (c),
3,4,5,6-Br_4 (d)

$L^{1\text{-}R}$

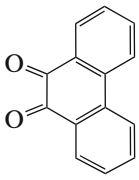

L^2

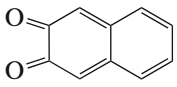

L^3

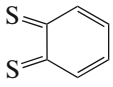

L^4

Scheme 1.

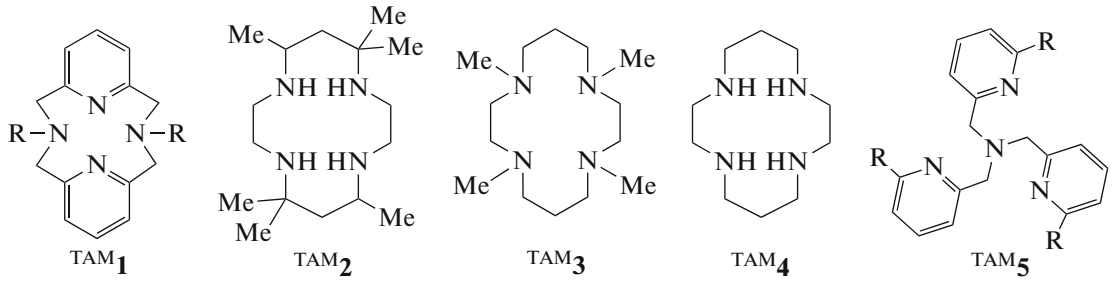

R = H, Me, *i*-Pr, *t*-Bu

Scheme 1. (Contd.).

STRUCTURES AND MAGNETIC BEHAVIOR OF THE COBALT AND IRON *o*-QUINONE COMPLEXES WITH TETRAAZAMACROCYCLIC LIGANDS

Pyridinophane derivatives. Tetraazamacrocyclic *N*,*N*'-dialkyl-2,11-diaza[3.3]-(2,6)pyridinophanes (pyridinophanes) (^{TAM}**1**-R_2) are capable of coordinating to metal centers remaining vacant two *cis* positions in the coordination sphere of the metal to form an octahedral environment [43]. For the cobalt compounds, the inclusion of *o*-quinone (dioxolene) into these positions results in the formation of the potential valence-tautomeric fragment [27]. However, contrary to expectations, the $[Co(^{TAM}\mathbf{1}\text{-}t\text{-}Bu_2)(L^{1b})]B(p\text{-}C_6H_4Cl)_4$ complex demonstrates the high-temperature (>400 K) SCO [40]. This compound is the only example of the cobalt *o*-quinone complex manifesting spin transitions via the SCO mechanism rather than the VT mechanism.

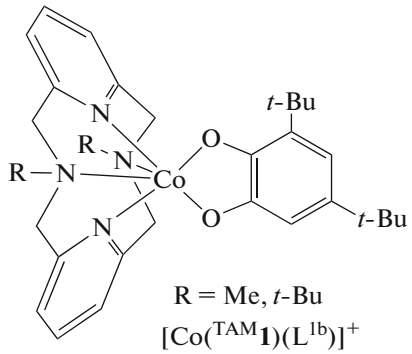

R = Me, *t*-Bu

$[Co(^{TAM}\mathbf{1})(L^{1b})]^+$

According to the magnetochemical measurements, ferromagnetic coupling is observed at room temperature between the low-spin cobalt(II) ion and the radical-anionic semiquinone (SQ) form of the redox-active ligand, but the incompleteness of the spin transition did not allow the study of the exchange interactions between the metal center and organic ligand [40]. The study of this compound using femtosecond electronic and IR vibrational nonstationary absorption spectroscopy showed that the selective photoexcitation of a solution of the complex at room temperature resulted in the superfast transformation of the low-spin (LS) fraction into the high-spin (HS) fraction [44]. On the contrary, the use of the macrocycle with methyl substituents at the nitrogen atoms favors the formation of the $[Co(^{TAM}\mathbf{1}\text{-}Me_2)(L^{1b})]^+$ complex existing in the $_{LS}Co^{III}Cat$ state (Cat is the dianionic catecholate form of the ligand) and exhibits no spin transitions.

For the purpose of fine tuning the ligand system of magnetically active compounds of this type, a series of complexes $[Co(^{TAM}\mathbf{1}\text{-}R_2)(L^{1b})]BPh_4$ (R = Me, Et, *i*-Pr, *t*-Bu) was synthesized, and their detailed study made it possible to establish the role of alkyl substituents of the pyridinophane ligand in the mechanism of magnetic bistability and its nature (SCO or VT) [45]. The $[Co(^{TAM}\mathbf{1}\text{-}i\text{-}Pr_2)(L^{1b})]BPh_4$ derivative was shown to undergo the thermally induced redox-isomeric rearrangement $[_{LS}Co^{III}Cat]^+ \rightleftarrows [_{HS}Co^{II}SQ]^+$, whereas a similar complex with $^{TAM}\mathbf{1}$-Et_2 exists predominantly in the diamagnetic state. The results of the quantum chemical simulation of these systems will be discussed in the second part of the present review.

In a wide temperature range, the iron complex with the *iso*-propyl pyridinophane derivative $[Fe(^{TAM}\mathbf{1}\text{-}i\text{-}Pr_2)(L^{1b})]BPh_4$ is presented by the isomer containing the high-spin trivalent metal ion [45]. Similar coordination compounds with the methyl-substituted pyridinophane macrocycle [41, 42] exist either as a dication with the $[_{LS}Fe^{III}(^{TAM}\mathbf{1}\text{-}Me_2)(SQ)]^{2+}$ structure ascribed to the compound on the basis of the data of Mössbauer spectroscopy, X-ray structure analysis, and magnetochemical measurements [42], or in the cationic form $[_{HS}Fe^{III}(^{TAM}\mathbf{1}\text{-}Me_2)(Cat)]^+$ [41].

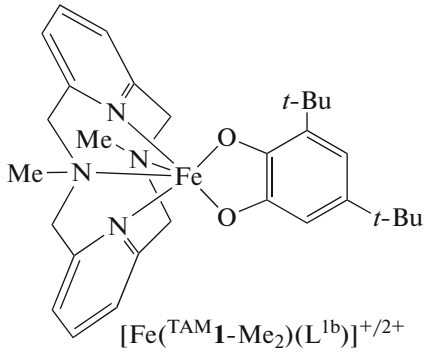

$[Fe(^{TAM}\mathbf{1}\text{-}Me_2)(L^{1b})]^{+/2+}$

In the $[_{LS}Fe^{III}(^{TAM}\mathbf{1}\text{-}Me_2)(SQ)]^{2+}$ compound, unpaired electrons of the low-spin metal ion and semiquinone are characterized by a strong antiferromagnetic coupling leading to diamagnetism. This compound is the first example of the isolated and structurally characterized complex bearing the low-spin trivalent iron ion and the SQ radical anion. The catalytic activity of the synthesized systems and their mimicry to dioxygenase are discussed [41, 42].

The SCO was observed in the iron(II) and iron(III) complexes with $^{TAM}\mathbf{1}\text{-}Me_2$ and in the iron(II) and cobalt(II) compounds with the *tert*-butyl derivative of pyridinophane $^{TAM}\mathbf{1}\text{-}t\text{-}Bu_2$ bearing the *N*-donor auxiliary ligands (bipyridyl (Bipy), 1,10-phenanthroline (Phen), and bipyrimidine (Bpym)) [46].

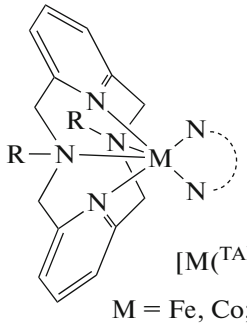

$[M(^{TAM}\mathbf{1})(L)]^{n+}$

M = Fe, Co; R = Me, *t*-Bu

L = Bipy, Phen, Bpym

Cyclam derivatives. Another well-known class of tetraazamacrocycles is presented by the cyclam derivatives: 5,7,7,12,14,14-hexamethyl-1,4,8,11-tetraazacyclotetradecane (**^{TAM}2**), 1,4,8,11-tetramethyl-1,4,8,11-tetraazacyclotetradecane (**^{TAM}3**), and 1,4,8,11-tetraazacyclotetradecane (**^{TAM}4**).

The iron(III) 3,5-di-*tert*-butyl catecholate complexes with $^{TAM}\mathbf{2}$, $^{TAM}\mathbf{4}$, and triazacyclononane were described [47]. The magnetic and EPR measurements indicate the presence of the trivalent metal ion in all compounds. The cobalt(II) and cobalt(III) semiquinone and catecholate complexes with $^{TAM}\mathbf{2}$ were synthesized and characterized in order to reveal conditions under which various oxidation states of the metals and ligands are stabilized [48].

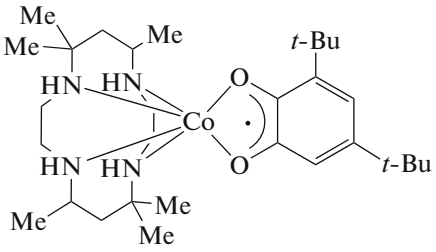

$[Co(^{TAM}\mathbf{2})(L^{1b})]^{2+}$

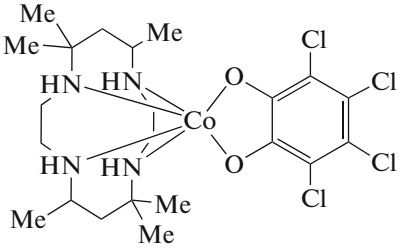

$[Co(^{TAM}\mathbf{2})(L^{1c})]^{+}$

The switching of the electronic states $_{LS}Co^{III}Cat$ and $_{HS}Co^{II}SQ$ of the quinone compounds with the general formula $[Co(^{TAM}\mathbf{2})(L^2)]Y$ (Y = PF_6, BPh_4, I) was studied [49]. These complexes undergo the VT transitions $[_{LS}Co^{III}(^{TAM}\mathbf{2})(Cat)]^+ \rightleftarrows [_{HS}Co^{II}(^{TAM}\mathbf{2})(SQ)]^+$, whose temperature varies depending on the counterions. An increase in the pressure results in the shift of the equilibrium toward the low-spin structure of a smaller volume.

The study of the $[Co(^{TAM}\mathbf{2})(L^2)]PF_6$ complex [49] was continued later [50]. The solvates considered [50]

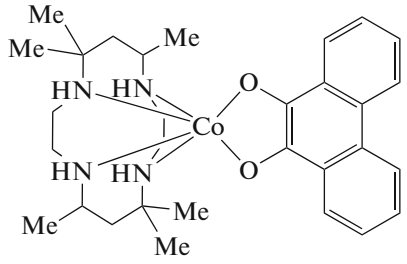

$[Co(^{TAM}\mathbf{2})(L^2)]^{+}$

demonstrate the photoinduced VT.

The cobalt compounds $[Co(^{TAM}\mathbf{3})(L^{1b})]PF_6$ and $[Co(^{TAM}\mathbf{3})(L^{2})]PF_6$ were synthesized [51] continuing the studies of the complexes with the cyclame derivatives. Both complexes exist in the form containing the high-spin cobalt(II) ion and SQ, unlike the derivative with $^{TAM}\mathbf{2}$ considered above. The ground triplet state of these compounds is formed due to the strong antiferromagnetic exchange between $_{HS}Co^{II}$ and SQ caused by the nonorthogonality of the magnetic orbitals.

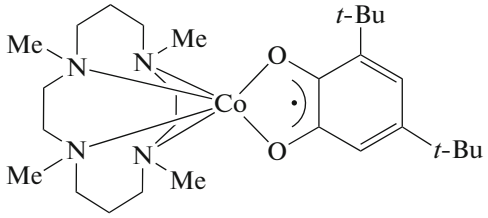

$[Co(^{TAM}\mathbf{3})(L^{1b})]^+$

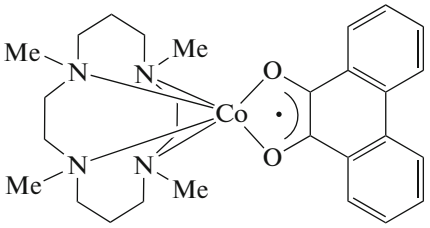

$[Co(^{TAM}\mathbf{3})(L^{2})]^+$

The photoinduced transformations of the $[Co(^{TAM}\mathbf{3})(L^{1b})]PF_6$ cobalt complex were characterized in the experiments using time-resolved spectroscopy [52]. It is shown that at least three different states ($_{HS}Co^{II}SQ$, $_{LS}Co^{III}Cat$, and $_{LS}Co^{II}SQ/_{IS}Co^{III}Cat$, where IS denotes the intermediate state) are involved in the $_{HS}Co^{II}SQ \rightarrow {}_{LS}Co^{III}Cat$ transition.

The earlier obtained data on the cobalt *o*-benzoquinone and 9,10-phenanthrenequinone complexes with the $^{TAM}\mathbf{2}$–$\mathbf{4}$ derivatives undergoing the VT transitions (where counterions are PF_6, I, and BPh_4; and solvents are H_2O, CH_2Cl_2, and $C_6H_5CH_3$) were generalized [53]. The dependences of the transition temperature on the counterion nature and the presence of the solvent molecules in the crystal were observed. The $_{LS}Co^{II}SQ$ electromer (along with the $_{LS}Co^{III}Cat$ and $_{HS}Co^{II}SQ$ isomers) is an important participant of the photocontrolled spin rearrangement. Antiferromagnetic exchange interactions were revealed between the paramagnetic centers. It was found later by the same group of authors that the replacement of dichloromethane by its deuterated analog in the $[Co(^{TAM}\mathbf{2})(L^{2})]^+$ compound was accompanied by a sharp change in the properties of the solvates and resulted in hysteresis [54]. A similar complex containing the tropolone anion was further synthesized and structurally characterized [55].

Tris(2-pyridylmethyl)amine derivatives. Tris(2-pyridylmethyl)amine ($^{TAM}\mathbf{5}$) formally has no macrocycle, but its behavior as a component of the coordination compounds with transition metals is close to that of the discussed class of organic N-donor ligands, and many cobalt and iron complexes demonstrating magnetically active properties with this were obtained ligand.

Cobalt complexes. The photoinduced (and thermally controlled) intramolecular electron transfer in the cobalt dioxolene complexes based on bis(6-methyl-(2-pyridylmethyl))(2-pyridylmethyl)amine ($^{TAM}\mathbf{5}$-Me_2) characterized by a long lifetime of the metastable electronic states was described [56]. As shown later [57], the $[Co(^{TAM}\mathbf{5}\text{-}Me_2)(L^{1b})]PF_6$ compound undergoes the VT with a critical temperature of 370 K.

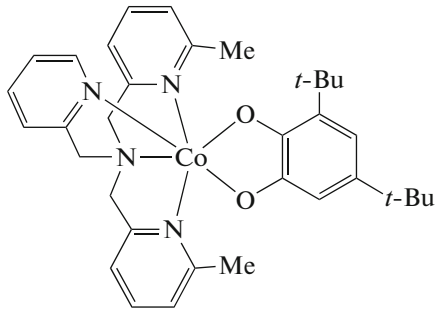

$[Co(^{TAM}\mathbf{5}\text{-}Me_2)(L^{1b})]^+$

The study of a series of the cobalt *o*-quinone complexes based on the tris(2-pyridylmethyl)amine ligands $[Co(^{TAM}\mathbf{5}\text{-}Me_n)(L^{1b})]PF_6 \cdot Solv$ (n = 0–3) shows that the steric hindrances created by the methyl substituents control the redox properties of the metal determining the charge distribution in the Co–L^{1b} fragment at room temperature [57]. The complexes in the solid state with n = 0, 1 represent the diamagnetic $_{LS}Co^{III}Cat$ derivatives, whereas the electronic structure $[_{HS}Co^{II}(^{TAM}\mathbf{5}\text{-}Me_3)(SQ)]^+$ was ascribed to the system containing three methyl groups in the tetraazamacrocycle. Compound $[Co(^{TAM}\mathbf{5}\text{-}Me_2)(L^{1b})]PF_6 \cdot C_2H_5OH$ experiences the entropy-controlled VT rearrangement at room temperature. The photoinduced VT in the complexes with n = 0–2 was observed on cooling. The obtained results demonstrate the efficiency of molecular design for the control of the relaxation properties of the photoinduced metastable states.

In continuation of the published works [56, 57], a similar cobalt complex with tetrachlorinated *o*-benzoquinone L^{1c} and $^{TAM}\mathbf{5}$-Me_3 was synthesized and stud-

ied using X-ray structure analysis, magnetic measurements, and electronic spectroscopy [58]. This system in the crystalline state was shown to undergo the VT at 300 K ($Co^{III}Cat \rightarrow Co^{II}SQ$), and the process in a solution is observed at 250 K. The thermodynamic parameters of the VT in the cationic cobalt dioxolene complexes (1 : 1) were determined for the first time and confirmed the entropy-controlled character of this process.

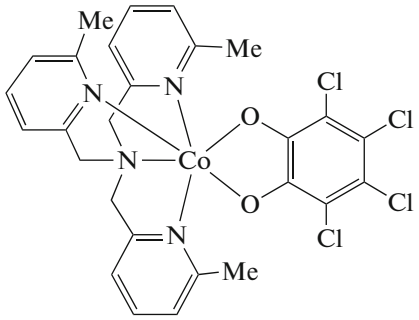

$[Co(^{TAM}\mathbf{5}\text{-}Me_3)(L^{1c})]^+$

The high sensitivity of the VT process to the crystalline lattice energy was demonstrated [56–58]. Various solvates (ethanol, toluene) of the earlier synthesized VT complex $[Co(^{TAM}\mathbf{5}\text{-}Me_n)(L^{1b})]PF_6$ were obtained to study this effect [59]. The influence of the solvent from which recrystallization is conducted on the thermally induced and photocontrolled VT was found. The role of the cobalt ion in the entropy- and photoinduced rearrangement of the VT exhibited by $[Co(^{TAM}\mathbf{5}\text{-}Me_2)(L^{1b})](PF_6) \cdot C_6H_5CH_3$ was evaluated using the X-ray absorption spectra [60]. The high stability and photostability make this compound to be a good candidate for the application in molecular devices. The influence of doping of $[Co(^{TAM}\mathbf{5}\text{-}Me_2)(L^{1b})]^+$ by the isomorphic zinc complex $[Zn(^{TAM}\mathbf{5}\text{-}Me_2)(L^{1b})](PF_6) \cdot C_6H_5CH_3$ on the entropy- and photoinduced VT transitions was studied [61]. The dilution by the diamagnetic metal complex was shown to exert almost no effect on the relaxation rate of the optically induced metastable high-spin state.

The data on the cobalt dioxolene complexes with the tetraazamacrocyclic ligands demonstrating valence tautomerism were generalized in the review [29]. It is shown that the relative stability of the redox isomers is determined by the temperature and irradiation with the light of the corresponding wavelength favors the transformation of the stable isomer into the metastable state.

The effect of the electrostatic field on the critical temperature of the VT rearrangement in the $[Co(^{TAM}\mathbf{5}\text{-}Me_2)(L^{1b})]PF_6$ complex was studied [62]. The obtained results demonstrate a new method for controlling the magnetism of the molecules and provide prospects for using the compounds with valence tautomerism for the development of molecular spintronic devices. The photoinduced VT in the $[Co(^{TAM}\mathbf{5}\text{-}Me_n)(L^{1b})]^+$ complexes was studied by transient IR spectroscopy [63].

The $[Co(^{TAM}\mathbf{5}\text{-}Me_3)(L^{1d})]^+$ complex capable of demonstrating the equilibrium $[_{LS}Co^{III}Cat]^+ \rightleftarrows [_{HS}Co^{II}SQ]^+$ was revealed by the quantum chemical simulation of a series of compounds $[Co(^{TAM}\mathbf{5}\text{-}Me_3)(L^{1a-d})]^+$ [38]. The assumption made on the basis of the calculations was confirmed by the subsequent synthesis and experimental studies (electronic spectroscopy, studies of magnetic susceptibility in the solid state and in a solution) of compounds $[Co(^{TAM}\mathbf{5}\text{-}Me_3)(L^{1d})]PF_6$ and $[Co(^{TAM}\mathbf{5}\text{-}Me_3)(L^{1d})]BPh_4$. The $[Co(^{TAM}\mathbf{5}\text{-}Me_3)(L^{1d})]^+$ complex in a solution was found to undergo the thermally controlled VT with the critical temperatures in a range of 291–359 K depending on the solvent. The $[Co(^{TAM}\mathbf{5}\text{-}Me_3)(L^{1d})]PF_6$ and $[Co(^{TAM}\mathbf{5}\text{-}Me_3)(L^{1d})]BPh_4$ complexes in the solid state exhibit unfinished VT transitions.

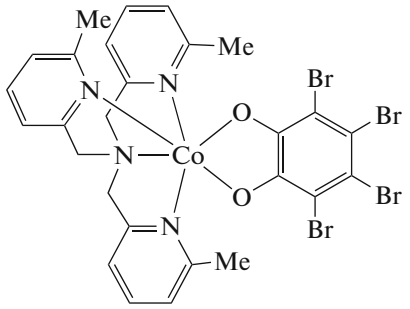

$[Co(^{TAM}\mathbf{5}\text{-}Me_3)(L^{1d})]^+$

The cationic cobalt complexes (counterions PF_6^- and BPh_4^-) with 2,3-dihydroxynaphthalene (L^3) were synthesized on the basis of $^{TAM}\mathbf{5}$ [64, 65]. The studies showed that the discussed systems contained the low-spin trivalent cobalt ion and the catecholate form of the redox ligand: the complexes are diamagnetic in a range of 2–380 K [66].

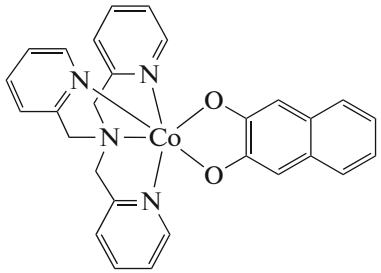

$[Co(^{TAM}\mathbf{5})(L^3)]^+$

Three cobalt 3,5-di-*tert*-butyl-*o*-quinone complexes were synthesized [67] with pyrazolyl-substituted tris(2-pyridylmethyl)amines: ^{TAM}**6** ($PzPy_2$ is (3,5-dimethyl-1*H*-pyrazolyl)-*N*,*N*-bis(2-pyridylmethyl)amine), ^{TAM}**7** (Pz_2Py is *N*,*N*-bis((3,5-dimethyl-1*H*-pyrazolyl)methyl)-*N*-(2-pyridylme-thyl)amine), and ^{TAM}**8** (Pz_3 is tris((3,5-dimethyl-1*H*-pyrazolyl)methyl)amine). Compound $[Co(^{TAM}\mathbf{6})\text{-}(L^{1b})]PF_6$ is diamagnetic, whereas the complexes with ^{TAM}**7** and ^{TAM}**8** are characterized by the ground high-spin state $[_{HS}Co^{II}(^{TAM}\mathbf{7}, \mathbf{8})(SQ)]PF_6$.

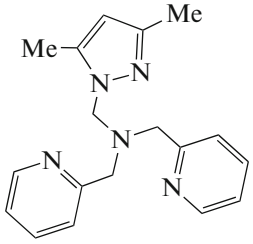

^{TAM}**6** ($PzPy_2$)

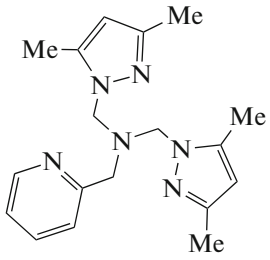

^{TAM}**7** (Pz_2Py)

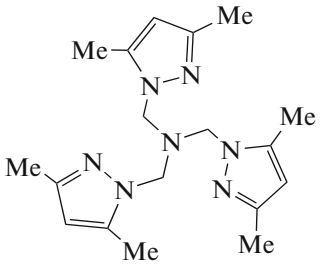

^{TAM}**8** (Pz_3)

The syntheses, crystal structures, and electrochemical behavior of nine new cobalt(III) complexes with tetrabromocatechol L^{1d} were reported [68]. Various bidentate bases (ethylenediamine, propylenediamine, 2-aminomethylpyridine, 8-aminoquinoline, and others), as well as the structural analog of ^{TAM}**5** tris(2-aminoethyl)amine (^{TAM}**9**), were used as nitrogen-containing ligands. All compounds in the ground state are diamagnetic, except for the derivative with 8-aminoquinoline capable of undergoing in a solution the thermally induced VT accompanied by a sharp change in the electronic spectra.

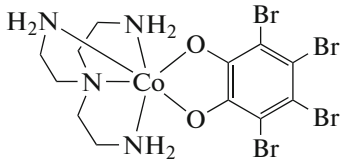

$[Co(^{TAM}\mathbf{9})(L^{1d})]^+$

Iron complexes. The first works in the iron *o*-quinone derivatives with the ^{TAM}**5** ligand appeared in the early 1990s [69, 70]. Compounds $[Fe(^{TAM}\mathbf{5})\text{-}(L^{1b})]BPh_4$ [69] and $[Fe(^{TAM}\mathbf{5}\text{-Me})(L^{1b})]ClO_4$ [70], as the majority of the complexes of this metal containing the redox ligands (L^1, L^4) and various tetraazamacrocycles (^{TAM}**5**-R (R = H, Me_n, Br, $((4\text{-}MeO)_2$, $4\text{-}Cl)_2$, $(4\text{-}NO_2)$, $(4\text{-}NO_2)_2$), ^{TAM}**10**–**17**) (Scheme 2), are considered as a functional model of the catechol dioxygenase enzyme [71–78].

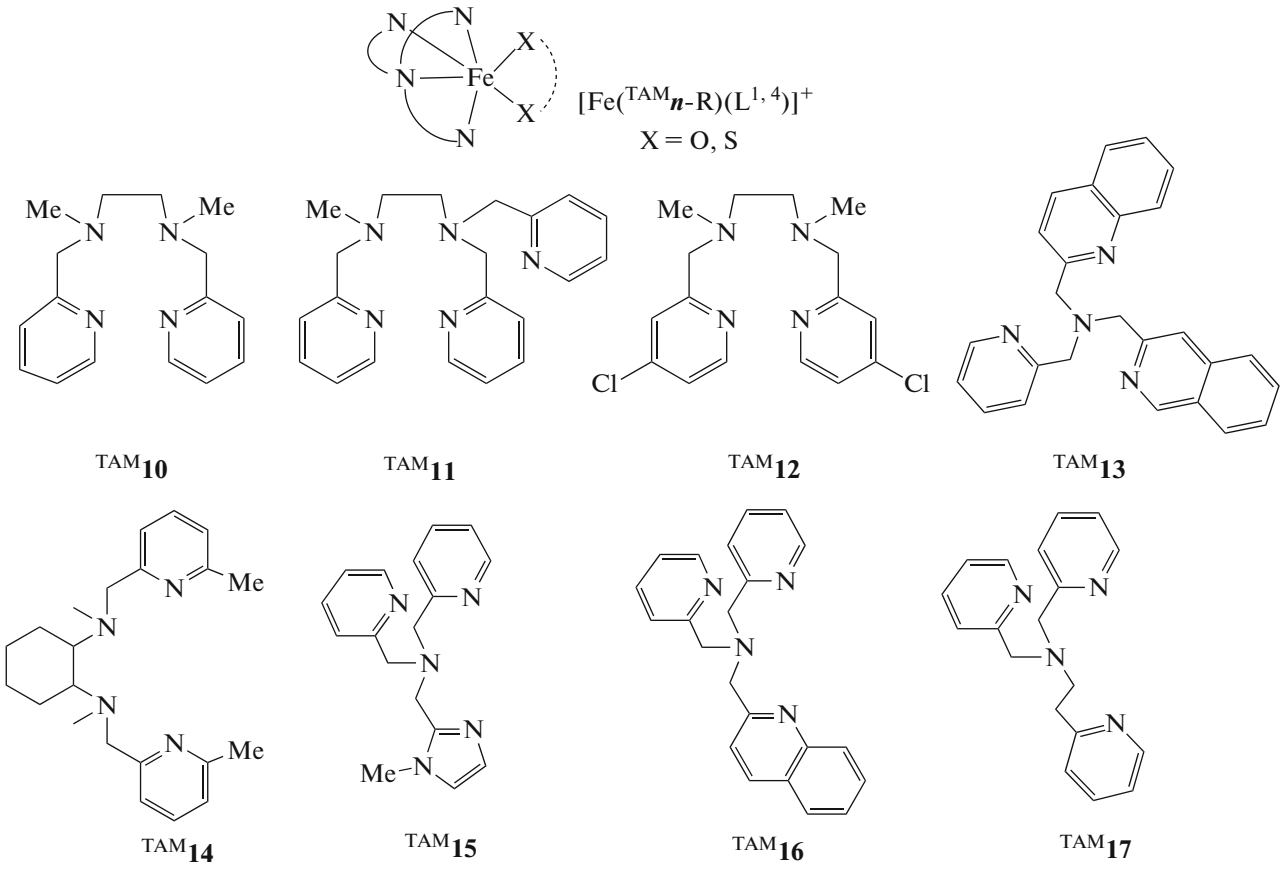

Scheme 2.

The synthesis of $[Fe(^{TAM}\mathbf{5})(L^{1a})]BPh_4$, which is a close analog of the previously described compound [69], was reported [79]. The SCO of trivalent iron ions $S = 1/2 \rightleftharpoons S = 5/2$ was found when studying the magnetic susceptibility in the solid state. This complex was studied in detail later [39]. The possibility of an equivalent mixture of the $Fe^{II}SQ$ and $Fe^{III}Cat$ configurations to exist in the ground and excited states is discussed taking into account the obtained experimental and theoretical data.

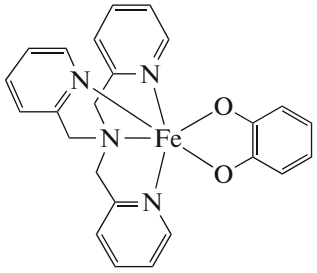

$[Fe(^{TAM}\mathbf{5})(L^{1a})]^+$

A series of compounds of the general formula $[Fe(^{TAM}\mathbf{5})(L^{1\text{-}R})]X$ (R = 4,5-$(NO_2)_2$, 3,4,5,6-Cl_4, 3-OMe, and 4-Me; X = BPh_4^-; NO_3^-; PF_6^-; and ClO_4^-) was obtained in the same research group [80]. Their magnetic behavior in the solid state shows the common features: the thermally controlled SCO occurs on the trivalent iron ion. The electronic configurations of the low-spin states are mainly determined by the chemical pressure experience by the complex under the lattice effect, which favors the mixing of $_{LS}Fe^{III}Cat$ and $_{LS}Fe^{II}SQ$ and allows one to expect both SCO and VT.

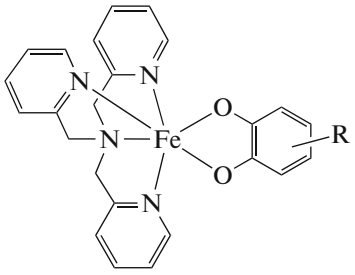

$[Fe(^{TAM}\mathbf{5})(L^{1\text{-}R})]^+$

R = 4,5-$(NO_2)_2$; 3,4,5,6-Cl_4; 3-OMe; 4-Me

The photophysical properties of the previously synthesized [39, 80] catecholate iron(III) complexes in the solid state were studied [81]. The photoexcitation processes initiating the LS → HS transition at low temperatures was examined. Later the electronic structures of these compounds were studied by the

EPR method [82]. The introduction of more electron-withdrawing substituents into the quinone ligand was found to enhance the *g*-tensor anisotropy due to an increase in the contribution of the Fe-Cat form [83].

Two polymorphs of the complex with tetrachlorocatechol $[Fe(^{TAM}\mathbf{5})(L^{1c})]PF_6$ were identified: monoclinic and orthorhombic [84]. Both polymorphs undergo the spin transition between the HS and LS states with a decrease in the temperature to 210 K.

The dynamics of spin state photoswitching in the $[Fe(^{TAM}\mathbf{5})(L^{1c})]^+$ cation with the SbF_6^- and PF_6^- anions was studied later using femtosecond optical spectroscopy in the pump-probe mode and picosecond X-ray diffraction [85, 86]. In both cases, three steps of the SCO are observed: at first excitation occurs to the state with the ligand–metal charge transfer and then relaxation to the metastable high-spin state occurs within 300 ns. This process is accompanied by an increase in the sizes of molecules resulting in an impact wave through the crystal due to which the crystal is extended within 10–10000 ns. Finally, the optical energy converts to the thermal energy favoring the conversion to the HS state within 50 μs. The $[Fe(^{TAM}\mathbf{5})(L^{1c})]SbF_6$ complex exhibits the incomplete thermal SCO $S = 1/2 \rightleftharpoons S = 5/2$ at 250 K [87]. The transition temperature increases by nearly 50 K upon the pressure application. The isolated iron tetrachlorocatecholate complexes with the diazepane derivatives were characterized by the spectral methods and electrochemistry, and their ability to imitate catechol dioxygenase was studied as for many complexes of those considered above [88].

The mononuclear iron(III) catecholate complex $[Fe(^{TAM}\mathbf{17})(L^{1a})]PF_6$ undergoing the incomplete SCO was synthesized and structurally characterized [89].

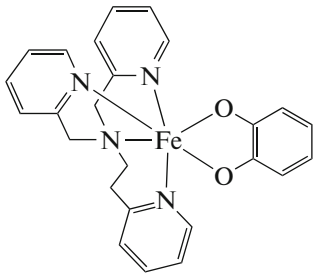

$[Fe(^{TAM}\mathbf{17})(L^{1a})]^+$

The mononuclear Fe(II) and Co(II) complexes with the redox-active ligand based on chloranilic acid also demonstrate the magnetically active properties [90]. It was shown that the spin state of the iron(II) complex can be controlled by the variation of the temperature (SCO at 251 K), pressure, and photoirradiation (LIESST at 42 K), whereas the cobalt(II) complex undergoes the redox-induced switching of the spin state to form the $_{LS}Co^{III}$ complex with the unchanged oxidation state of the redox-active ligand.

Metal *o*-quinone complexes functionalized by radical fragments. Presently, this type of metal complexes attracts special attention due to three spin carriers in them: metal ion, semiquinone, and paramagnetic substituent. The cycle of the works [91–96] is devoted to the synthesis and study of the complexes of the first transition series with *o*-quinone ligands containing the nitronylnitroxyl (NN) radical linked to the *o*-benzoquinone ring directly or through the bridging groups. The most part of these compounds applied as auxiliary ligands contains hydro(tris(3-cumenyl-5-methylpyrazolyl)borate) [92, 94–96].

It was found that the cobalt bis-*o*-NN-semiquinone complex $[Co(L^{1b}\text{-Ph-NN})_2(Bipy)]$, whose coordination sphere is built up to an octahedron by bipyridyl, can undergo VT [93].

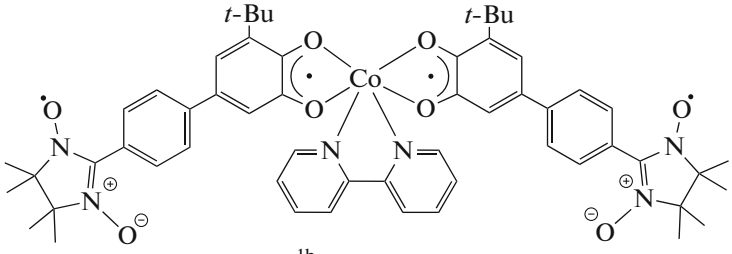

$Co(L^{1b}\text{-Ph-NN})_2(Bipy)$

The cobalt(III) compounds $Co(L^{1b}\text{-NN})_2(Py)_2$ and $Co(L^{1b}\text{-Ph-NN})_2(Py)_2$ were studied [94]. The authors emphasize that strong ferromagnetic exchange interactions are observed in the SQ–NN pair of all studied systems [91–96].

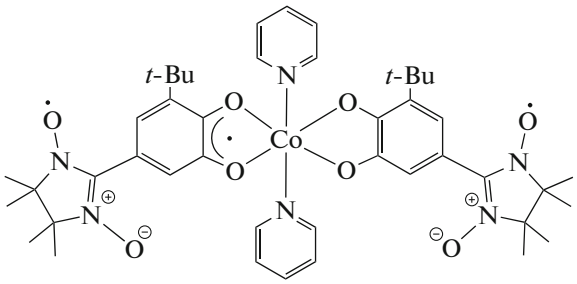

$Co(L^{1b}\text{-}NN)_2(Py)_2$

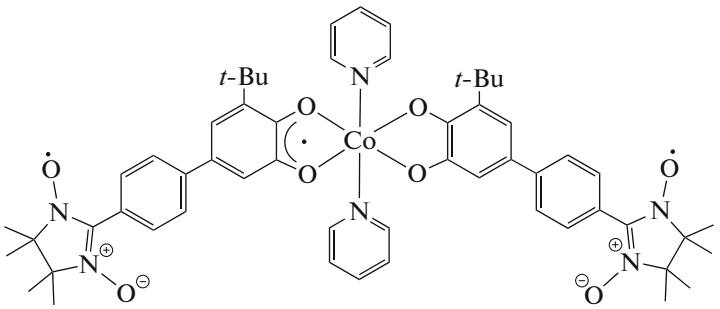

$Co(L^{1b}\text{-}Ph\text{-}NN)_2(Py)_2$

The iron(III) complex with NN-catechol containing the *tert*-butyl substituent in position 3 and tetraazamacrocycle ^{TAM}**5** was reported in 2015 [97]. Compound $[Fe^{III}(^{TAM}\mathbf{5})(L^{1b}\text{-}NN)]BPh_4$, whose structure was determined by X-ray diffraction analysis and Mössbauer spectroscopy, exhibits weak the ferromagnetic exchange interactions Fe(III)–NN and undergoes SCO.

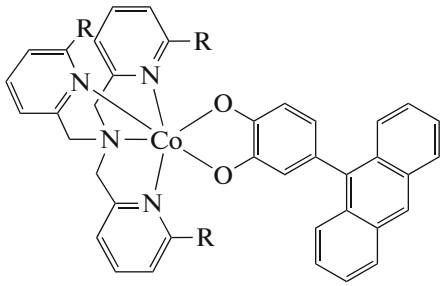

$[Co(^{TAM}\mathbf{5}\text{-}Me_n)(L^1\text{-}Ac)]^+$

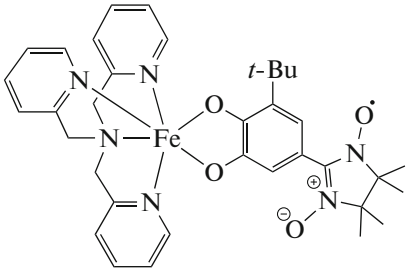

$[Fe(^{TAM}\mathbf{5})(L^{1b}\text{-}NN)]^+$

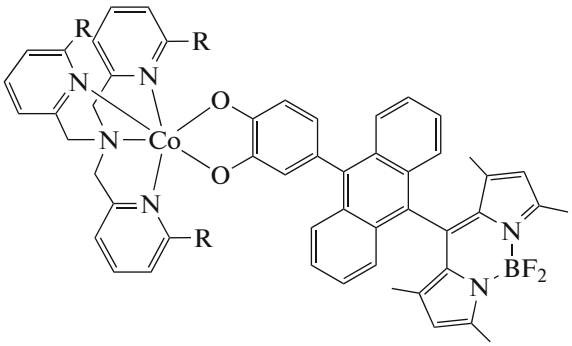

$[Co(^{TAM}\mathbf{5}\text{-}Me_n)(L^1\text{-}Ac\text{-}BODIPY)]^+$

The cobalt complexes with quinones functionalized by anthracene and tris(2-pyridylmethyl)amine derivatives $[Co^{TAM}\mathbf{5}\text{-}Me_n)(L^1\text{-}Ac)]PF_6$ ($n = 0$–3) were synthesized [98]. Compound $[Co(^{TAM}\mathbf{5})(L^1\text{-}Ac)]PF_6$ in the solid state exists in the diamagnetic form ($_{LS}Co^{III}Cat$), whereas the $[Co(^{TAM}\mathbf{5}\text{-}Me_n)(L^1\text{-}Ac)]PF_6$ ($n = 3$) complex bearing three methyl groups at the nitrogen atoms of the tetraazamacrocyclic ligand contains the high-spin cobalt(II) ion and the semiquinone form of the redox-active ligand ($_{HS}Co^{II}SQ$). The systems with $n = 1, 2$ demonstrate the VT, including the photoinduced VT (at 5 K). In continuation of this trend, similar complexes $[Co(^{TAM}\mathbf{5}\text{-}Me_n)(L^1\text{-}Ac\text{-}BODIPY)]PF_6$ (n = 0, 3) containing borodipyrromethane (BODIPY) in the redox-active ligand were synthesized [99]. It was shown that BODIPY exerted no effect on the spin state of the complex.

Thus, the *o*-quinone metal complexes with the tetraazamacrocyclic ligands are objects of many-sided experimental studies. At the same time, methods of quantum chemistry should be used because of difficulties appeared in determining the electronic and spin states of the isomers and revealing "structure–properties" regularities.

THEORETICAL SIMULATION OF THE ELECTRONIC STRUCTURES AND MAGNETIC PROPERTIES OF THE COBALT AND IRON *o*-BENZOQUINONE COMPLEXES WITH TETRAAZAMACROCYCLIC LIGANDS

The quantum chemical simulation of the mononuclear cobalt and iron *o*-quinone complexes with tetradentate macrocyclic nitrogen-containing bases was

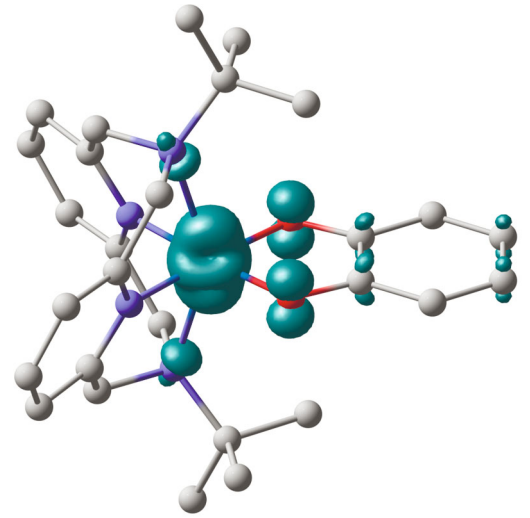

$_{LS}Co^{II}SQ$

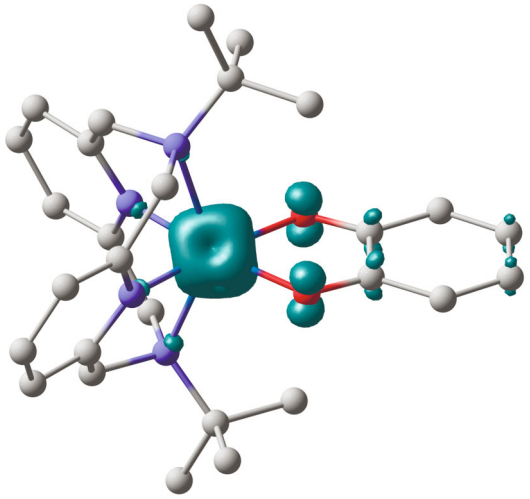

$_{HS}Co^{II}SQ$

Fig. 1. Calculated spin density distribution in the $_{LS}Co^{II}SQ$ and $_{HS}Co^{II}SQ$ electromers of the $[Co(^{TAM}\mathbf{1}\text{-}t\text{-}Bu_2)(L^{1a})]^+$ complex. Here and in Figs. 3–7, hydrogen atoms are omitted for clarity.

performed in order to study the magnetic behavior of the earlier synthesized compounds [40, 45, 49, 53–59] and to reveal the structural parameters responsible for the possibility of occurring the mechanisms of spin state switching in the systems considered. All calculations were performed using the Gaussian 09 program [100] by the density functional theory (DFT) method with the UTPSSh functional [101, 102] and extended 6-311++G(d,p) basis set, a combination of which correctly reproduces the energy and magnetic characteristics of the cationic complexes exhibiting the magnetic bistability mechanisms [12, 45, 103–108]. According to the calculation results obtained in this approximation for the experimentally studied systems, the SCO on the iron ion occurs at $\Delta E_{HS\text{-}LS} < 11$ kcal/mol [103, 104], the SCO on the cobalt ion occurs at $\Delta E_{HS\text{-}LS} < 5$ kcal/mol, and the VT in the complexes with the cobalt ion is observed at $\Delta E_{HS\text{-}LS} < 10$ kcal/mol [109, 110]. The stationary points were localized on the potential energy surface (PES) by the full optimization of the molecular structure geometry with checking the DFT stability of the wave function and calculating the force constants. Since neither the Mulliken, nor NBO charges give a valid representation about the oxidation state of the central ion in the complexes with the redox-active ligands, it seems reasonable to estimate this parameter by the number of unpaired electrons on the metal atom and characteristic bond lengths of the ligands. The exchange interaction parameters (J, cm^{-1}) were calculated in terms of the broken symmetry (BS) formalism [111] using the method of the generalized spin projection proposed by Yamaguchi [112]. The detailed information about the procedure of DFT studies of the transition metal complexes with redox-active ligands was presented [113].

Cobalt complexes with the pyridinophane derivatives. According to the calculations, the ground state of the cationic $[Co(^{TAM}\mathbf{1}\text{-}t\text{-}Bu_2)(L^{1a})]^+$ complex based on *o*-benzoquinone and the di-*tert*-butyl derivative of pyridinophane is the electronic isomer (electromer [114]) $_{LS}Co^{II}SQ$ on the triplet PES [109].

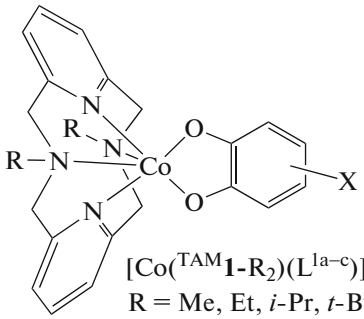

$[Co(^{TAM}\mathbf{1}\text{-}R_2)(L^{1a–c})]^+$
R = Me, Et, *i*-Pr, *t*-Bu
X = 3,5-*t*-Bu, 3,4,5,6-Cl

The spin density is observed on the metal and on the oxygen atoms and adjacent carbon atoms (Fig. 1), indicating the low-spin state of the two-charge cobalt ion and semiquinone form of the ligand. The geometric characteristics of the $_{LS}Co^{II}SQ$ structure [109] are well consistent with the X-ray structure analysis data for the complex at 200 K [40, 44]. The ferromagnetic coupling of unpaired electrons ($J = 579$ cm^{-1}) was predicted in the $_{LS}Co^{II}SQ$ isomer [109], which confirms the assumption [40, 44] about strong exchange interactions of the ferromagnetic type in this form of the complex.

The high-spin isomer $_{HS}Co^{II}SQ$ on the quintet PES is destabilized over $_{LS}Co^{II}SQ$ by 6.2 kcal/mol [109], which makes it possible to expect the incomplete transition of $[Co(^{TAM}\mathbf{1}\text{-}t\text{-}Bu_2)(L^{1a})]^+$ to the high-spin state. This conclusion is consistent with the

results of the magnetochemical measurements of the complex [40, 44]. The calculation of the BS state indicates the antiferromagnetic exchange ($J = -46$ cm^{-1}) [109] between unpaired electrons of semiquinone and the high-spin cobalt ion. The results are consistent with the moderate antiferromagnetic interactions obtained in the complexes of high-spin Co(II) with the semiquinone ligands [51].

The destabilization of the $_{LS}Co^{III}Cat$ structure over $_{LS}Co^{II}SQ$, which is the ground state of the complex, does not allow the thermally initiated intramolecular redox process to occur.

The inclusion of the tetra(*p*-chlorophenyl)borate counterion into the calculation scheme led to a decrease in the difference in energies between the low-spin isomers $_{LS}Co^{III}Cat$ and $_{LS}Co^{II}SQ$. The latter, as in the considered above cationic complex, is the ground state and characterized by strong ferromagnetic interactions of spins of unpaired electrons [110]. The optimum difference in energies between the $_{LS}Co^{II}SQ$ and $_{HS}Co^{II}SQ$ structures provides the possibility of switching of the magnetic properties of the [Co(^{TAM}**1**-*t*-Bu$_2$)(L^{1a})]B(*p*-C$_6$H$_4$Cl)$_4$ compound via spin crossover. The isomers containing the three-charge cobalt ion and catecholate form of *o*-quinone is destabilized, because short Co–N coordination bonds cannot be formed due to steric hindrances created by the *tert*-butyl groups of the nitrogen-containing macrocyclic ligand.

The replacement of bulky substituents in the pyridinophane ligands by methyl groups with accounting for the counterion stabilizes the $_{LS}Co^{III}Cat$ isomer on the singlet PES [109]. Therefore, the [Co(^{TAM}**1**-Me$_2$)(L^{1a})]BF$_4$ complex is diamagnetic, which is completely consistent with experiment [40, 44].

The compounds bearing ethyl and isopropyl groups were studied by the DFT method to elucidate the influence of alkyl substituents on the magnetic properties of the complexes of the considered type [45]. The calculations of the [Co(^{TAM}**1**-Et$_2$)(L^{1b})]BPh$_4$ complex indicate that the low-spin form $_{LS}Co^{III}Cat$ is energetically preferable. The $_{HS}Co^{II}SQ$ electromer is destabilized over the ground state by 10.9 kcal/mol suggesting the incomplete VT transition. This conclusion is confirmed by an increase in the effective magnetic moment in the discussed compound at the temperature higher than 340 K [45]. As in the above considered complexes with ^{TAM}**1**-*t*-Bu$_2$ and ^{TAM}**1**-Me$_2$, the high-spin electromer is characterized by the antiferromagnetic coupling of spins of unpaired electrons of the metal ion and SQ.

A different result is predicted for the [Co(^{TAM}**1**-*i*-Pr$_2$)(L^{1b})]BPh$_4$ complex. The difference in energies between the ground state $_{LS}Co^{III}Cat$ and the high-spin isomer $_{HS}Co^{II}SQ$ (4.6 kcal/mol) favors the VT to occur, which is observed experimentally [45].

A comparison of the energy characteristics of the electromers of the cobalt complexes considered above showed (Fig. 2) that an increase in the size of the alkyl substituent in the tetraazamacrocycle (Me → Et → *i*-Pr) favored bringing together the energies of the $_{HS}Co^{II}SQ$ and $_{LS}Co^{III}Cat$ isomers and resulted in favorable conditions for the VT rearrangements to occur in the [Co(^{TAM}**1**-*i*-Pr$_2$)(L^{1b})]BPh$_4$ complex. The inversion of the relative energies is observed with the further increase in the substituent bulkiness (compound [Co(^{TAM}**1**-*t*-Bu$_2$)(L^{1f})]B(*p*-C$_6$H$_4$Cl)$_4$): the $_{LS}Co^{II}SQ$ electromer is stabilized over $_{LS}Co^{III}Cat$ by 4.7 kcal/mol thus providing conditions for the SCO transition rather than VT. Thus, the variation of alkyl substituents in ^{TAM}**1** allows one to control the relative stability of the electromeric forms of the complexes and, as a consequence, the type of the mechanism of spin state switching.

According to the calculation results, the electron-withdrawing substituents in *o*-benzoquinone enhance the stability of the $_{LS}Co^{III}Cat$ state, favoring the facilitation of the intramolecular electron transfer: the energy characteristics of the electromers of the complex with tetrachloro-*o*-benzoquinone [Co(^{TAM}**1**-Me$_2$)(L^{1c})]$^+$ allow one to expect the VT rearrangement [110]. As in the compounds considered above, the exchange between spins of unpaired electrons of the semiquinone radical and high-spin metal ion of the $_{HS}Co^{II}SQ$ isomer is antiferromagnetic ($J = -62$ cm^{-1}) [110].

The $_{LS}Co^{II}SQ$ electromer containing the ligand in the SQ form and low-spin divalent cobalt ion is the most stable form of [Co(^{TAM}**1**-*t*-Bu)(L^{1c})]$^+$. Strong ferromagnetic interactions were predicted between unpaired electrons of the SQ form and cobalt ion. The high-spin structure $_{HS}Co^{II}SQ$ is destabilized over the ground state by 5.8 kcal/mol, which allows one to expect the thermally controlled SCO complicated by the antiferromagnetic exchange in the high-spin isomer ($J = -22$ cm^{-1}) in this complex [110].

Thus, the character of exchange interactions in the considered cobalt *o*-benzoquinone complexes with the ^{TAM}**1** derivatives is determined by the electronic configuration of the metal atom and is independent of substituents in the ligands: a strong ferromagnetic exchange was predicted for the isomers with low-spin Co(II), whereas a moderate antiferromagnetic exchange was predicted for the structures with high-spin Co(II).

Cobalt complexes with tris(2-pyridylmethyl)amines. The difference in energies between the $_{LS}Co^{III}Cat$ and $_{HS}Co^{II}SQ$ isomers of the cationic cobalt complex [Co(^{TAM}**5**)(L^{1a})]$^+$ makes it possible to predict the

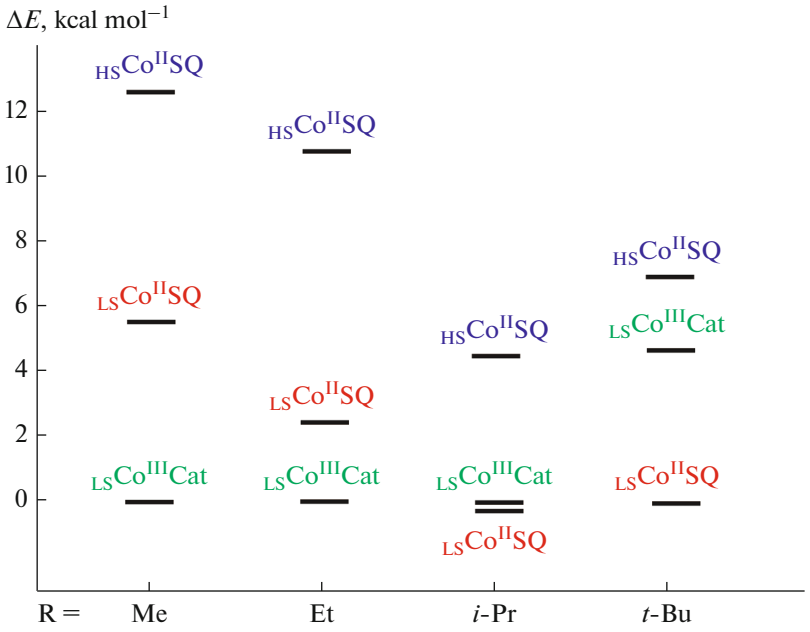

Fig. 2. Plot of the relative energies of the electromers of the cobalt *o*-quinone complexes with *N*-dialkyl derivatives ^{TAM}**1**.

redox-isomeric rearrangement, which does not agree with the experimental data [57] indicating that the diamagnetic state prevails in a wide temperature range. The inclusion of the hexafluorophosphate anion into the calculation scheme results in the destabilization of the high-spin electromer $_{HS}Co^{II}SQ$ and blocking the VT in the $[Co(^{TAM}\mathbf{5})(L^{1a})]PF_6$ compound [110, 113]. The exchange between SQ and the cobalt ion is strongly ferromagnetic in character regardless of the spin state of the metal ($_{LS}Co^{II}SQ$ and $_{HS}Co^{II}SQ$) and the presence of a counterion.

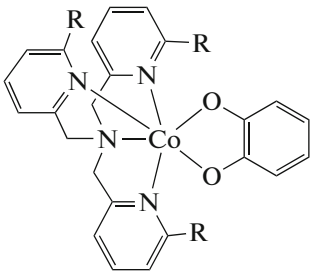

$[Co(^{TAM}\mathbf{5}\text{-}R_3)(L^{1a})]^+$

R = H, Me

The results of the calculation of the electromers of the cobalt complex $[Co(^{TAM}\mathbf{5}\text{-}Me_2)(L^{1a})]PF_6$ with the tris(2-pyridylmethyl)amine ligand containing two methyl groups in position 6 of the pyridine rings well reproduce the experimental data [57], indicating that the VT rearrangement $_{LS}Co^{III}Cat \rightleftarrows {}_{HS}Co^{II}SQ$ occurs at room temperature. The substituents in the nitrogen-containing ligand exert no substantial effect on the strength of the ferromagnetic exchange interactions [110].

The introduction of an additional methyl group favors the stabilization of the paramagnetic $_{HS}Co^{II}SQ$ form of the $[Co(^{TAM}\mathbf{5}\text{-}Me_3)(L^{1a})]PF_6$ complex containing the high-spin cobalt ion and semiquinone, the exchange between which is also ferromagnetic (J = 197 cm^{-1}).

Different exchange interactions in the high-spin states of the complexes with the pyridinophane and tris(2-pyridylmethyl)amine ligands are due to the orientation of the magnetic orbitals. As can be seen from Fig. 3, a significant overlapping favoring the appearance of the antiferromagnetic exchange channel is observed in compound $[Co(^{TAM}\mathbf{1}\text{-}Me_2)(L^{1a})]^+$, and the orthogonality of the magnetic orbitals of the $[Co(^{TAM}\mathbf{5})(L^{1a})]^+$ complex results in the ferromagnetic coupling of spins of unpaired electrons of the metal and SQ radical anion.

Thus, in the studied cobalt *o*-benzoquinone complexes with the ^{TAM}**1** and ^{TAM}**5** derivatives, the possibility of spin state switching, the type of the process mechanism, and the character of exchange interactions are determined by the nature of the tetraazamacrocyclic ligand and substituents in *o*-quinone. The insertion of alkyl groups creating steric hindrances in the coordination site makes it possible to control the redox states of the complexes. Taking into account the counterions in the calculations and the presence of electron-withdrawing substituents enhance the stability of the low-spin isomers bearing the three-charge metal ion and the catecholate form of the ligand. The considered systems demonstrate the importance of

including outer-sphere counterions into the calculation scheme when studying the coordination compounds of transition metals with the redox-active ligands.

Iron complexes with the pyridinophane derivatives. The previous experimental studies of the iron *o*-quinone complexes with the pyridinophane macrocycle are devoted to establishing their catalytic activity and the ability to imitate the behavior of the dioxygenase enzyme [41, 42]. The magnetic properties of these compounds were not studied. In order to reveal the possibility of the magnetic bistability mechanisms to take place, the calculations of the monocationic iron *o*-quinone complexes with *N*,*N*'-dimethyl-2,11-diaza[3.3]-(2,6)pyridinophane $[Fe(^{TAM}\mathbf{1}\text{-}Me_2)(L^{1a})]^+$ were performed [115].

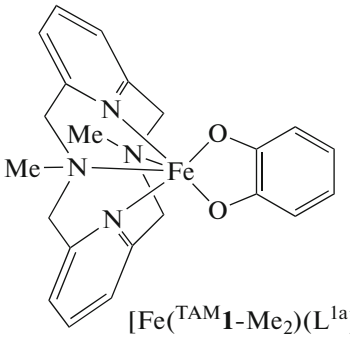

$[Fe(^{TAM}\mathbf{1}\text{-}Me_2)(L^{1a})]^+$

An analysis of the calculated geometric characteristics and spin density distribution indicate the simultaneous presence of two low-spin forms $_{LS}Fe^{III}Cat$ and $_{LS}Fe^{II}SQ$. The presence of four unpaired electrons on the metal and a significant amount of the spin density on the oxygen and carbon atoms of *o*-benzoquinone makes it possible to ascribe the $_{HS}Fe^{II}SQ$ state to the electromer on the sextet PES. This state contains the two-charge iron ion in the high-spin state and semiquinone radical between which strong ferromagnetic exchange interactions were predicted (J = 185 cm^{-1}). The calculated difference in energies between the isomers of the $[Fe(^{TAM}\mathbf{1}\text{-}Me_2)(L^{1a})]^+$ complex is 10.6 kcal/mol, which allows the thermally initiated spin transition in the complex to occur [115].

The calculation of the neutral $[Fe(^{TAM}\mathbf{1}\text{-}Me_2)(L^{1a})]PF_6$ complex indicates that the low- and high-spin electromers contain the catecholate form of the redox ligand and three-charge iron ions. Taking into account the counterion is not accompanied by a change in the energy characteristics of the $_{LS}Fe^{III}Cat$ and $_{HS}Fe^{III}Cat$ isomers (ΔE = 10.6 kcal/mol), which suggests that the thermally controlled spin crossover into which the $_{IS}Fe^{III}Cat$ electromer with the intermediate spin state of the metal (ΔE = 8.5 kcal/mol) can be involved [115]. Thus, the results of the quantum-chemical calculations of the $[Fe(^{TAM}\mathbf{1}\text{-}Me_2)(L^{1a})]PF_6$ complex indicate that the complex manifests the magnetically active properties, and this can stimulate experimental investigations of this compound.

$[Co(^{TAM}\mathbf{1}\text{-}Me_2)(L^{1a})]^+$

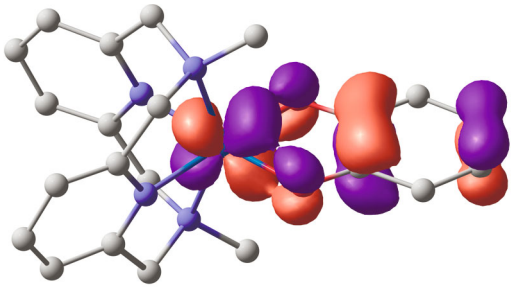

$[Co(^{TAM}\mathbf{5})(L^{1a})]^+$

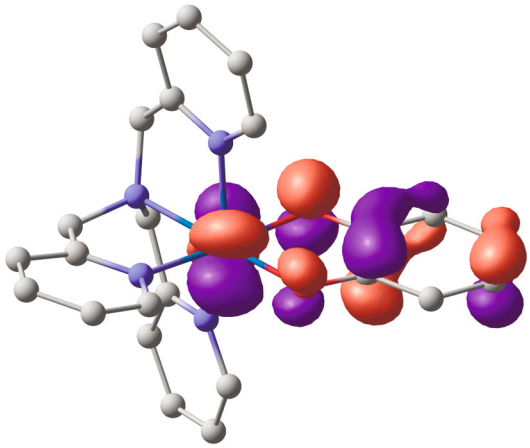

Fig. 3. Magnetic orbitals of the $_{HS}Co^{II}SQ$ electromers of the $[Co(^{TAM}\mathbf{1}\text{-}Me_2)(L^{1a})]^+$ and $[Co(^{TAM}\mathbf{5})(L^{1a})]^+$ complexes.

The dicationic iron *o*-benzoquinone complexes with *N*-dialkylpyridinophane derivatives were considered further [116].

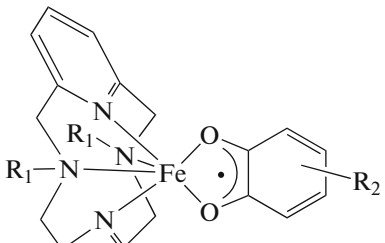

$[Fe(^{TAM}\mathbf{1}\text{-}R_1)(L^1)]^{2+}$
R_1 = Me, *t*-Bu; R_2 = H, Cl

According to the calculations [116], the ground state of $[Fe(^{TAM}\mathbf{1}\text{-}Me_2)(L^{1a})]^{2+}$ is the low-spin $_{LS}Fe^{III}SQ$ isomer on the triplet PES including the trivalent metal ion and SQ form of the redox-active ligand (Fig. 4). The calculated bond lengths in the coordination site and benzoquinone ring correlate

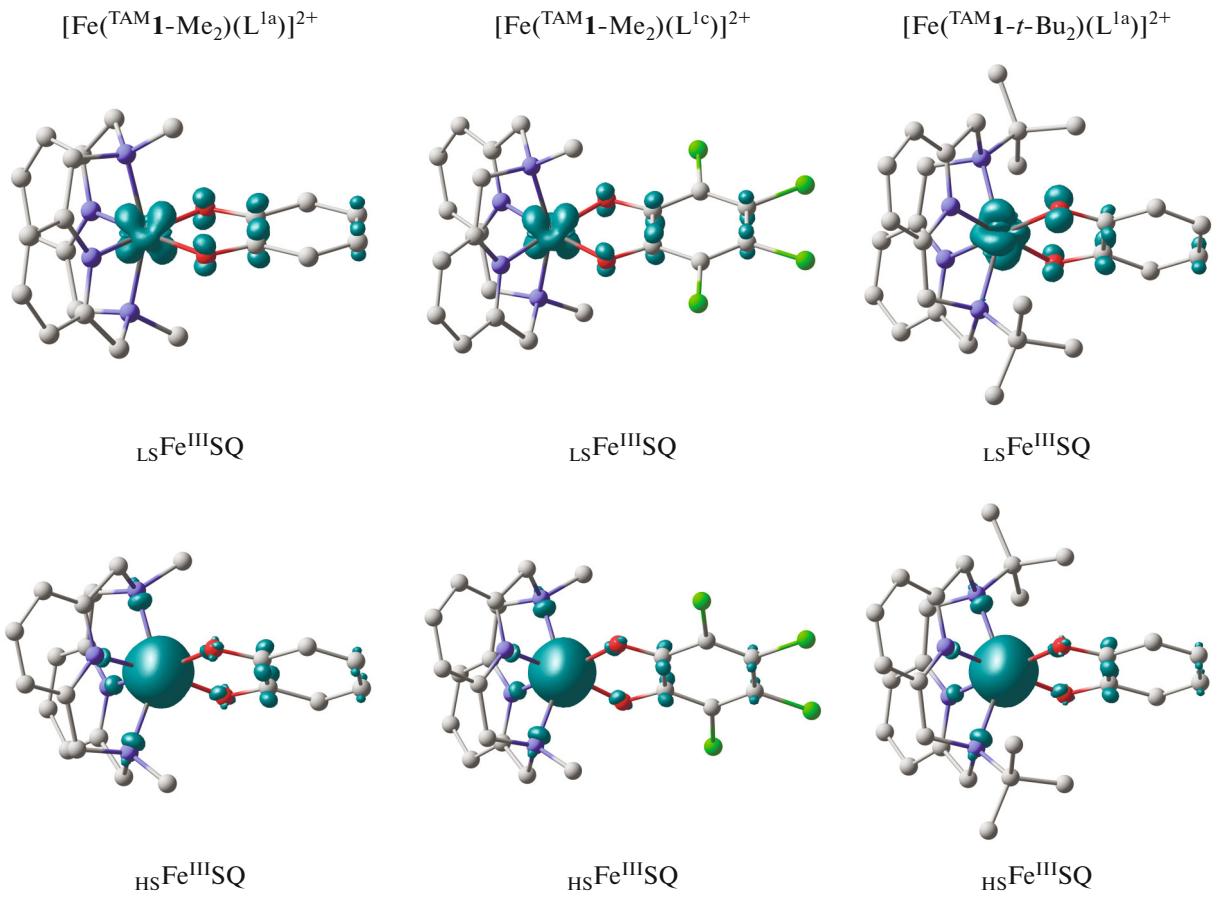

Fig. 4. Calculated spin density distribution in the electromers of the dicationic complexes $[Fe(^{TAM}\mathbf{1}\text{-}Me_2)(L^{1a})]^{2+}$, $[Fe(^{TAM}\mathbf{2}\text{-}Me_2)(L^{1c})]^{2+}$, and $[Fe(^{TAM}\mathbf{1}\text{-}t\text{-}Bu_2)(L^{1a})]^{2+}$.

well with the values found by X-ray structure analysis [42]. Strong exchange interactions of the antiferromagnetic character were predicted for the discussed electromer [116], which is also consistent with the experimental data indicating diamagnetism of the complex [42]. The $_{HS}Fe^{III}SQ$ isomer containing the high-spin trivalent iron ion and semiquinone (between which a strong antiferromagnetic coupling was predicted) was localized on the septet PES. The relative energy of the electromers (ΔE = 14.4 kcal/mol) does not allow one to expect that the thermally initiated spin transition would occur in the $[Fe(^{TAM}\mathbf{1}\text{-}Me_2)(L^{1a})]^{2+}$ complex.

Similar results were obtained for the $[Fe(^{TAM}\mathbf{1}\text{-}Me_2)(L^{1c})]^{2+}$ derivatives. The calculations showed that the chlorine substituents in the radical ligand exerted no substantial effect on the energy and magnetic characteristics of the electromers of this complex [116]. The destabilization of the $_{HS}Fe^{III}SQ$ isomer over the low-spin structure of $_{LS}Fe^{III}SQ$ by 14.1 kcal/mol indicates that the high-spin state is thermally unattainable. In the electromer on the doublet PES, strong antiferromagnetic exchange interactions would favor diamagnetism of the complex in a wide temperature range.

As can be shown earlier [40, 45, 109, 110], the bulky substituents at the donor atoms of the tetraazamacrocyclic ligands impede the formation of the low-spin isomer, which shortens the difference in energies between the electromers to the values favoring the occurrence of the thermally controlled SCO. The calculations of the $[Fe(^{TAM}\mathbf{1}\text{-}t\text{-}Bu_2)(L^{1a})]^{2+}$ complex showed that the replacement of the methyl substituents at the nitrogen atoms of the pyridinophane ligand by *tert*-butyl groups was accompanied by changes in the geometric and energy characteristics of the electromers [116]. The predicted narrowing of the energy gap between the $_{LS}Fe^{III}SQ$ and $_{HS}Fe^{III}SQ$ electromers to 7.7 kcal/mol allows the spin transition on the iron ion to occur. Thus, the quantum chemical simulation of the dicationic iron *o*-semiquinone complexes with the pyridinophane derivatives showed that the electron-withdrawing groups in the radical ligand exerted no significant effect on the magnetic properties of the considered coordination compounds, whereas the variation of the substituents at the nitro-

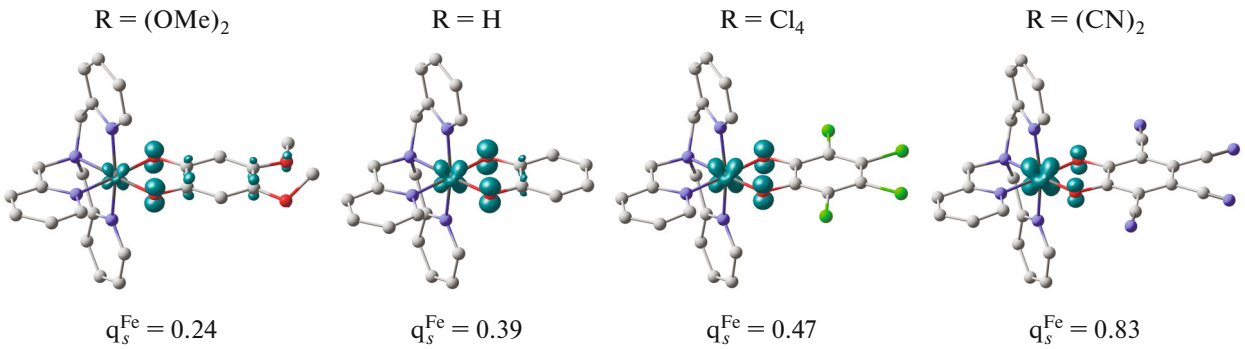

Fig. 5. Calculated spin density distribution in the low-spin electromers of the $[Fe(^{TAM}\mathbf{5})(L^{1e,a,c,f})]^+$ complexes.

gen atoms of the tetradentate base is accompanied by a change in the geometric and energy characteristics of the isomers. This allows one to expect the thermally initiated SCO in the dicationic iron *o*-benzoquinone complex with *N*,*N*'-di-*tert*-butyl-2,11-diaza[3.3]-(2,6)pyridinophane.

Iron complexes with tris(2-pyridylmethyl)amines. According to the calculations of the cationic and electroneutral iron complexes with tris(2-pyridylmethyl)amine $[Fe(^{TAM}\mathbf{5})(L^{1a})]^+$ and $[Fe(^{TAM}\mathbf{5})(L^{1a})]PF_6$, the ground state is presented by the structures on the doublet PES in which a mixture of the configurations ${}_{LS}Fe^{III}Cat + {}_{LS}Fe^{II}SQ$ including the low-spin metal ions in various oxidation states is expected [115], which agrees with the previous assumptions [39]. The minima on the sextet PES correspond to the ${}_{HS}Fe^{II}SQ$ electromers containing the two-charge iron ion in the high-spin state and the semiquinone radical between which strong ferromagnetic exchange interactions were predicted. The energy characteristics of the isomers of the $[Fe(^{TAM}\mathbf{5})(L^{1a})]^+$ and $[Fe(^{TAM}\mathbf{5})(L^{1a})]PF_6$ complexes allow one to expect the thermally initiated spin transition.

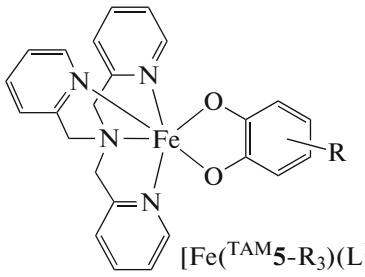

$[Fe(^{TAM}\mathbf{5}\text{-}R_3)(L^{1a,c,e,f})]^+$
R = H, Cl_4, $(OMe)_2$, CN_4

The consideration of the $[Fe(^{TAM}\mathbf{5})(L^{1c})]PF_6$ complex with *o*-chloranil showed that the presence of the chlorine substituents resulted in the stabilization of the structures bearing the catecholate form of the redox-active ligand and three-charge iron ion [115]. The calculated difference in energies between the low- and high-spin isomers agrees with the SCO that occurs in this compound [80]. Therefore, the presence of halogens in *o*-benzoquinone does not affect the occurrence of spin transitions of the $[Fe(^{TAM}\mathbf{5})(L^{1c})]^+$ and $[Fe(^{TAM}\mathbf{5})(L^{1c})]PF_6$ complexes.

The spin density distribution in the low-spin isomers of the $Fe(^{TAM}\mathbf{5})$ complexes with *o*-benzoquinones containing the electron-active substituents is presented in Fig. 5. Two powerful electron-donating OMe groups (complex $[Fe(^{TAM}\mathbf{5})(L^{1e})]^+$) stabilize the divalent state of iron, which is indicated by the almost complete absence of the spin density on the metal ion. By contrast, four electron-withdrawing cyano groups (compound $[Fe(^{TAM}\mathbf{5})(L^{1f})]^+$) transform iron into the oxidation state +3. The spin density delocalization predicted by the calculations for the experimentally studied systems $[Fe(^{TAM}\mathbf{5})(L^{1a})]^+$ and $[Fe(^{TAM}\mathbf{5})(L^{1c})]^+$ is intermediate between the cases considered above. On the one hand, this result is completely consistent with the data of magnetochemical and Mössbauer studies indicating a high lability of electronic states of this type of the complexes. On the other hand, this result demonstrates the influence of the modification of the *o*-benzoquinone ligand on the occurrence of the VT or SCO.

Thus, the quantum chemical study of the iron dioxolene complexes with the tris(2-pyridylmethyl)amine ligands showed the ability of these compounds to demonstrate spin crossover. The substituents in *o*-benzoquinone were found to exert no substantial effect on the difference in energies between the low- and high-spin states of the complex, but the substituents play the determining role in the stabilization of the electronic configurations. The substituents with the pronounced electron-withdrawing properties in the benzoquinone ring favor the shift of the electron density from the iron ion and an increase in the stability of the structures containing the three-charge metal ion and the dianionic form of the redox-active ligand. At the same time, the electron-donating groups in *o*-quinone stabilize the $Fe^{II}SQ$ electromers.

Cobalt and iron *o*-quinone complexes functionalized by radical fragments. The mutual influence of acene

and *o*-benzoquinone groups was studied in the work [99] devoted to the synthesis and investigation of the mononuclear cobalt complexes with the anthracene fragment. The polycyclic group in the discussed systems is diamagnetic due to a short lifetime of the excited triplet state. An increase in the number of conjugated rings to five facilitates the transformation of acenes into the paramagnetic form.

The computer simulation of the $[M(^{TAM}\mathbf{1}\text{-}t\text{-}Bu_2)(L^5)]^+$ and $[M(^{TAM}\mathbf{1}\text{-}t\text{-}Bu_2)(L^6)]^+$ (M = Co, Fe) compounds was performed to combine in one molecule of the metal-containing center, which is potentially capable of undergoing the thermally initiated spin transition, and the polyacene linker group, whose singlet–triplet transitions are controlled by photoirradiation. The coordination sphere of the metal in these complexes is built up by *N*,*N*'-di-*tert*-butyl-2,11-diaza[3.3]-(2,6)pyridinophane. The radical group in the $[M(^{TAM}\mathbf{1}\text{-}t\text{-}Bu_2)(L^5)]^+$ compounds is presented by linear heptacene. As follows from the earlier obtained calculation results [117], the energy gap between the singlet (biradical) and triplet forms of heptacene does not exceed 7 kcal/mol, which favors heptacene transition to the high-spin state under irradiation. A specific feature of the $[M(^{TAM}\mathbf{1}\text{-}t\text{-}Bu_2)(L^6)]^+$ compounds is the presence in polycyclic hydrocarbon of the terminal five-membered rings favoring, according to the experimental and theoretical data [117–119], the stabilization of the triplet state of this acene already for five condensed cycles.

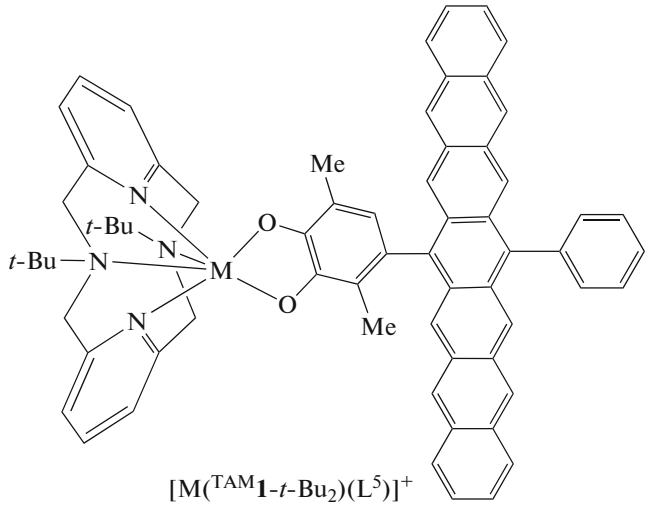

$[M(^{TAM}\mathbf{1}\text{-}t\text{-}Bu_2)(L^5)]^+$

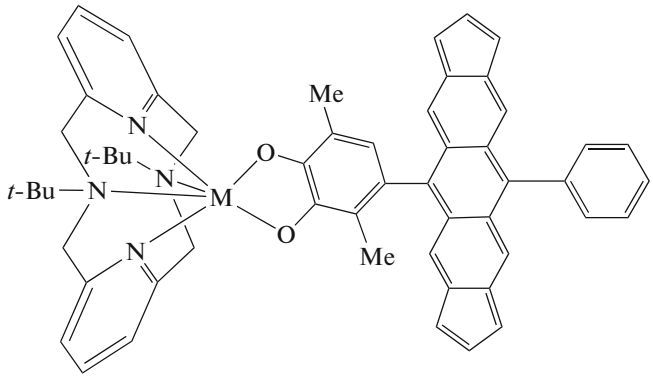

$[M(^{TAM}\mathbf{1}\text{-}t\text{-}Bu_2)(L^6)]^+$

According to the obtained results regardless of the type of terminal rings and metal ion, the acene linker is stabilized as a singlet biradical characterized by the strong antiferromagnetic coupling [120]. The spin density in heptacene (compounds $[M(^{TAM}\mathbf{1}\text{-}t\text{-}Bu_2)(L^5)]^+$ (M = Co, Fe)) is concentrated in the central part of the linker on the opposite carbon atoms of the polyaromatic chain (Figs. 6, 7). A different spin density distribution was found in the $[Co(^{TAM}\mathbf{1}\text{-}t\text{-}Bu_2)(L^6)]^+$ and $[Fe(^{TAM}\mathbf{1}\text{-}t\text{-}Bu_2)(L^6)]^+$ complexes: the paramagnetic centers of the polycyclic fragment of these compounds are located on the carbon atoms of the terminal five-membered cycles.

The ground state in the cobalt complexes is the $_{LS}Co^{II}SQ–[C]_n–[C]_n$ electromer containing the low-spin two-charge metal ion and semiquinone, which agrees with the earlier studies of the mononuclear cobalt *o*-benzoquinone compounds with $^{TAM}\mathbf{1}\text{-}t\text{-}Bu_2$ [40, 45, 110]. The high-spin isomers with the electronic configuration $_{HS}Co^{II}SQ–[C]_n–[C]_n$ are localized on the septet PES. The energy gap between the low- and high-spin states of the $[Co(^{TAM}\mathbf{1}\text{-}t\text{-}Bu_2)(L^5)]^+$ and $[Co(^{TAM}\mathbf{1}\text{-}t\text{-}Bu_2)(L^6)]^+$ complexes is 6.3 and 6.2 kcal/mol, respectively, indicating that the thermally initiated SCO can occur [120]. The exchange interactions between unpaired electrons of semiquinones and metal ions are of the same character as those in the previously considered mononuclear compounds with pyridinophane ligands [40, 45, 110]: the strong ferromagnetic coupling was predicted for the low-spin $_{LS}Co^{II}–SQ$ fragment, whereas the spins of unpaired electrons in the $_{HS}Co^{II}–SQ$ pair interact antiferromagnetically.

The data obtained suggest that the length and structure of the acene fragment in the $[Co(^{TAM}\mathbf{1}\text{-}t\text{-}Bu_2)(L^5)]^+$ and $[Co(^{TAM}\mathbf{1}\text{-}t\text{-}Bu_2)(L^6)]^+$ complexes exert no substantial effect on the possibility of manifesting the rearrangements accompanied by spin state switching. At the same time, the biradical linker favors the formation of additional exchange channels $_{LS}Co^{II}–[C]_n$, $_{HS}Co^{II}–[C]_n$, and $SQ–[C]_n$ [120], whose characteristics can be controlled by the variation of the rotation angle of the quinone ring over the polycyclic chain [121].

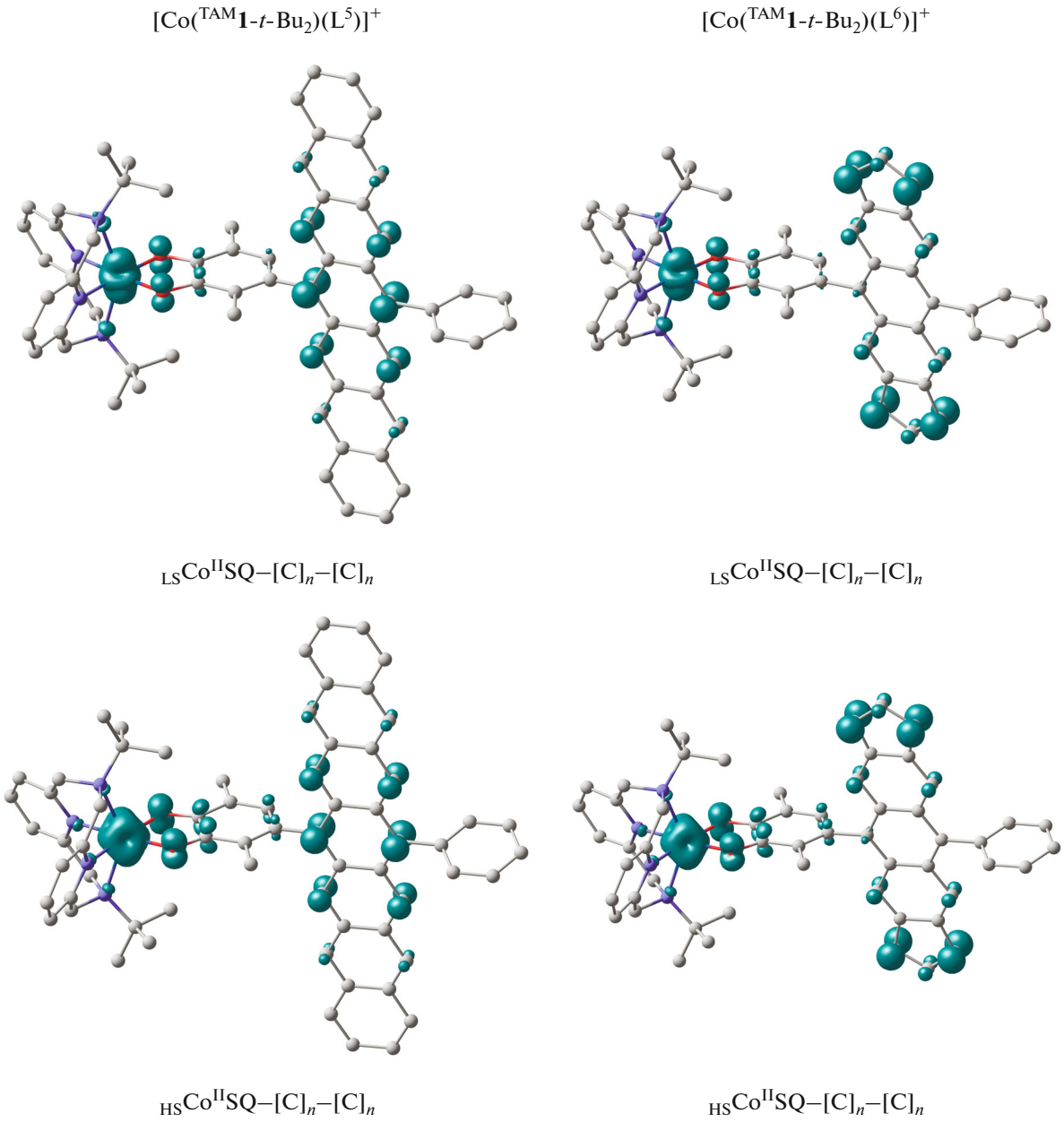

Fig. 6. Calculated spin density distribution in the electromers of the $[Co(^{TAM}\mathbf{1}\text{-}t\text{-}Bu_2)(L^5)]^+$ and $[Co(^{TAM}\mathbf{1}\text{-}t\text{-}Bu_2)(L^6)]^+$ complexes.

In the similarly built up iron complexes $[Fe(^{TAM}\mathbf{1}\text{-}t\text{-}Bu_2)(L^5)]^+$ and $[Fe(^{TAM}\mathbf{1}\text{-}t\text{-}Bu_2)(L^6)]^+$, the electromers found on the quartet and octet PES contain the trivalent metal ions and catecholate form of the redox-active ligand (Fig. 7). As in the dicationic derivative $[Fe(^{TAM}\mathbf{1}\text{-}t\text{-}Bu_2)(L^{1a})]^{2+}$ considered above [116], the *tert*-butyl groups at the nitrogen atoms of the tetradentate macrocycle create optimum conditions for the stabilization of both electromeric forms. The differences in energies between the ${}_{LS}Fe^{III}Cat–[C]_n–[C]_n$ and ${}_{HS}Fe^{III}Cat–[C]_n–[C]_n$ states do not exceed 5 kcal/mol, which allows one to expect that the SCO would occur in the $[Fe(^{TAM}\mathbf{1}\text{-}t\text{-}Bu_2)(L^5)]^+$ and $[Fe(^{TAM}\mathbf{1}\text{-}t\text{-}Bu_2)(L^6)]^+$ complexes. The replacement of the *tert*-butyl substituents by methyl groups results in the stabilization of the low-spin state and blocking the spin transition. The obtained result confirms the substantial influence of the alkyl groups at the nitrogen atoms of the tetraazamacrocyclic ligand on the energy characteristics of these systems.

According to the calculated exchange parameters, antiferromagnetic interactions of a moderate strenght are expected between the paramagnetic centers local-

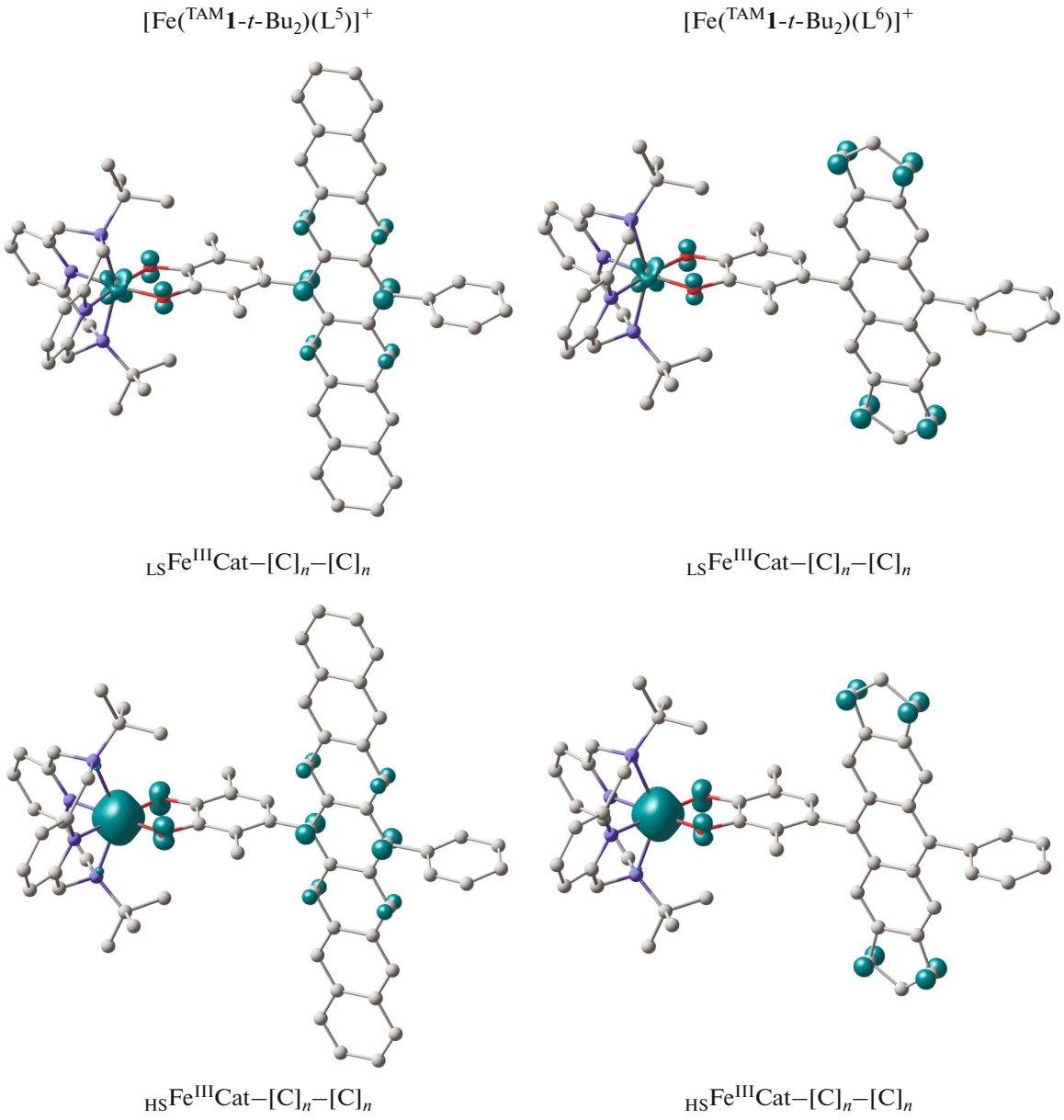

Fig. 7. Calculated spin density distribution in the electromers of the $[Fe(^{TAM}\mathbf{1}\text{-}t\text{-}Bu_2)(L^5)]^+$ and $[Fe(^{TAM}\mathbf{1}\text{-}t\text{-}Bu_2)(L^6)]^+$ complexes.

ized on the iron ions (both in the low- and high-spin states) and polyaromatic hydrocarbon.

Thus, the quantum chemical calculations showed that the complex formation of cobalt and iron ions with *o*-benzoquinone ligands containing acene groups can lead to the system manifesting the thermally switchable spin states of the metal-centered fragments and photocontrolled singlet–triplet transitions of the polycyclic radical. The magnetic bistability mechanism of these complexes is determined by the nature of the tetraazamacrocyclic ligand, whereas the presence of additional exchange channels depends on the structure of the acene chain.

To conclude, the reviewed results of the experimental and theoretical studies of the metal *o*-quinone complexes with the tetraazamacrocyclic ligands indicate wide prospects of the practical application of this class of magnetically active compounds in molecular electronics and spintronics. The magnetic behavior of the experimentally studied systems was explained by the quantum chemical calculations performed by us, since it is difficult to unambiguously interpret the data of their magnetochemical studies because of a combination of spin transitions and exchange interactions. The dependences of the spin transitions, type of the mechanisms of these rearrangements, and character of

exchange interactions on the nature of the tetradentate nitrogen-containing bases and substituents in the redox-active fragment were found in the studied series of the cobalt and iron *o*-quinone complexes with the tetraazamacrocyclic ligands. The functionalization of the structural motif $[M(^{TAM}\boldsymbol{n})(L^n)]^{+/2+}$, for example, by the introduction of radical groups into the *o*-quinone fragment or the construction of binuclear structures provides broad prospects for the preparation of new magnetically active systems. The systematic computer simulation of the electronic structures and magnetic properties of the compounds of the type considered allowed new complexes potentially capable of exhibiting magnetic bistability mechanisms to be proposed. The use of the known compounds as building blocks in the design of new molecules makes it possible to expect the successful synthesis of the predicted systems.

FUNDING

This work was supported by the Russian Science Foundation, project no. 19-73-00090.

CONFLICT OF INTEREST

The authors declare that they have no conflicts of interest.

REFERENCES

1. Poddel'sky, A.I., Cherkasov, V.K., and Abakumov, G.A., *Coord. Chem. Rev.*, 2009, vol. 253, nos. 3–4, p. 291.
2. Teki, Y., Shirokoshi, M., Kanegawa, S., and Sato, O., *Eur. J. Inorg. Chem.*, 2011, no. 25, p. 3761.
3. Alley, K.G., Poneti, G., Aitken, J.B., et al., *Inorg. Chem.*, 2012, vol. 51, no. 7, p. 3944.
4. Dai, J., Kanegawa, S., Li, Z., et al., *Eur. J. Inorg. Chem.*, 2013, no. 24, p. 4150.
5. Witt, A., Heinemann, F.W., Sproules, S., and Khusniyarov, M.M., *Chem.-Eur. J.*, 2014, vol. 20, no. 35, p. 11149.
6. Madadi, A., Itazaki, M., Gable, R.W., et al., *Eur. J. Inorg. Chem.*, 2015, no. 30, p. 4991.
7. Witt, A., Heinemann, F.W., and Khusniyarov, M.M., *Chem. Sci.*, 2015, vol. 6, no. 8, p. 4599.
8. Drath, O., Gable, R.W., Moubaraki, B., et al., *Inorg. Chem.*, 2016, vol. 55, no. 9, p. 4141.
9. Zolotukhin, A.A., Bubnov, M.P., Bogomyakov, A.S., et al., *Inorg. Chim. Acta*, 2016, vol. 440, p. 16.
10. Drath, O., Gable, R.W., Poneti, G., et al., Cryst. *Growth Des.*, 2017, vol. 17, no. 6, p. 3156.
11. Zolotukhin, A.A., Bubnov, M.P., Arapova, A.V., et al., *Inorg. Chem.*, 2017, vol. 56, no. 24, p. 14751.
12. Piskunov, A.V., Pashanova, K.I., Ershova, I.V., et al., *J. Mol. Struct.*, 2018, vol. 1165, p. 51.
13. Starikova, A.A. and Minkin V.I., *Russ. Chem. Rev.*, 2018, vol. 87, no. 11, p. 1049.
14. Piskunov, A.V., Pashanova, K.I., Bogomyakov, A.S., et al., *Dalton Trans.*, 2018, vol. 47, no. 42, p. 15049.
15. Zolotukhin, A.A., Bubnov, M.P., Cherkasov, V.K., et al., *Russ. J. Coord. Chem.*, 2018, vol. 44, no. 4, p. 272. https://doi.org/10.1134/S1070328418040085
16. Piskunov, A.V., Pashanova, K.I., Ershova, I.V., et al., *Russ. Chem. Bull.*, 2019, vol. 68, no. 4, p. 757.
17. Protasenko, N.A., Poddel'sky, A.I., Bogomyakov, A.S., et al., *Inorg. Chim. Acta*, 2019, vol. 489, p. 1.
18. Cherkasova, A.V., Kozhanov, K.A., Zolotukhin, A.A., et al., *Russ. J. Coord. Chem.*, 2019, vol. 45, no. 7, p. 489. https://doi.org/10.1134/S1070328419070029
19. Ershova, I.V., Smolyaninov, I.V., Bogomyakov, A.S., et al., *Dalton Trans.*, 2019, vol. 48, no. 28, p. 10723.
20. Zolotukhin, A.A., Bubnov, M.P., Bogomyakov, A.S., et al., *Inorg. Chim. Acta*, 2019, vol. 488, p. 278.
21. Hauser, A., *Coord. Chem. Rev.*, 1991, vol. 111, p. 275.
22. *Spin Crossover in Transition Metal Compounds*, I–III. *Topics in Curr. Chem.*, vols. 233–235. Gütlich P. and Goodwin H.A., Eds., Berlin–Heidelberg: Springer, 2004.
23. *Spin-Crossover Materials: Properties and Applications*, Halcrow M.A., Ed., Chichester: Wiley, 2013.
24. Minkin, V.I. and Starikov, A.G., *Russ. Chem. Bull.*, 2015, vol. 64, no. 3, p. 475.
25. Buchanan, R.M. and Pierpont, C.G., *J. Am. Chem. Soc.*, 1980, vol. 102, no. 15, p. 4951.
26. Evangelio, E. and Ruiz-Molina, D., *Eur. J. Inorg. Chem.,* 2005, no. 15, p. 2957.
27. Tezgerevska, T., Alley, K.G., and Boskovic, C., *Coord. Chem. Rev.*, 2014, vol. 268, p. 23.
28. Minkin, V.I., *Russ. Chem. Bull.*, 2008, vol. 57, no. 4, p. 687.
29. Dei, A. and Sorace, L., *Appl. Magn. Reson.*, 2010, vol. 38, no. 2, p. 139.
30. *Molecular Switches*, Eds. Feringa, B.L. and Browne, W.R., Weinheim: Wiley-VCH, 2011.
31. Troiani, F. and Affronte, M., *Chem. Soc. Rev.*, 2011, vol. 40, no. 6, p. 3119.
32. Aromí, G., Aguilá, D., Gamez, P., et al., *Chem. Soc. Rev.*, 2012, vol. 41, no. 2, p. 537.
33. Sato, O., *Nature Chem.,* 2016, vol. 8, no. 7, p. 644.
34. Khusniyarov, M.M., C*hem.-Eur. J.*, 2016, vol. 22, no. 43, p. 15178.
35. Demir, S., Jeon, I.-R., Long, J.R., and Harris, T.D., *Coord. Chem. Rev.*, 2015, vols. 289–290, p. 149.
36. Senthil Kumar, K and Ruben, M., *Coord. Chem. Rev.*, 2017, vol. 346, p. 176.
37. Drath, O. and Boskovic, C., *Coord. Chem. Rev.*, 2018, vol. 375, p. 256.
38. Gransbury, G.K., Boulon, M.-E., Petrie, S., et al., *Inorg. Chem.*, 2019, vol. 58, no. 7, p. 4230.
39. Simaan, A.J., Boillot, M.-L., Carrasco, R., et al., C*hem.-Eur. J.*, 2005, vol. 11, no. 6, p. 1779.
40. Graf, M., Wolmershäuser, G., Kelm, H., et al., *Angew. Chem., Int. Ed. Engl.*, 2010, vol. 49, no. 5, p. 950.
41. Koch, W.O. and Krüger, H.J., *Angew. Chem., Int. Ed. Engl.*, 1995, vol. 34, nos. 23–24, p. 2671.

42. Koch, W.O., Schünemann, V., Gerdan, M., et al., C*hem.-Eur. J.*, 1998, vol. 4, no. 7, p. 1255.
43. Kruüger, H.J., *Chem. Ber.*, 1995, vol. 128, no. 6, p. 531.
44. Rupp, F., Chevalier, K., Graf, M., et al., C*hem.-Eur. J.*, 2017, vol. 23, no. 9, p. 2119.
45. Tezgerevska, T., Rousset, E., Gable, R.W., et al., *Dalton Trans.*, 2019, vol. 48, no. 31, p. 11674.
46. Krüger, H.-J., *Coord. Chem. Rev.*, 2009, vol. 253, nos. 19–20, p. 2450.
47. Dei, A., Gatteschi, D., and Pardi, L., *Inorg. Chem.*, 1993, vol. 32, no. 8, p. 1389.
48. Benelli, C., Dei, A., Gatteschi, D., and Pardi, L., *Inorg. Chim. Acta*, 1989, vol. 163, no. 1, p. 99.
49. Caneschi, A., Dei, A., Fabrizi, De., Biani, F., et al., C*hem.-Eur. J.*, 2001, vol. 7, no. 18, p. 3926.
50. Carbonera, C., Dei, A., Sangregorio, C., and Letard, J.-F., *Chem. Phys. Lett.*, 2004, vol. 396, nos. 1–3, p. 198.
51. Caneschi, A., Dei, A., Gatteschi, D., and Tangoulis, V., *Inorg. Chem.*, 2002, vol. 41, no. 13, p. 3508.
52. Neuwahl, F.V.R., Righini, R., and Dei, A., *Chem. Phys. Lett.*, 2002, vol. 352, nos 5-6, p. 408.
53. Bencini, A., Caneschi, A., Carbonera, C., et al., *J. Mol. Struct.*, 2003, vol. 656, nos. 1–3, p. 141.
54. Cador, O., Dei, A., and Sangregorio, C., *Chem. Commun.*, 2004, no. 6, p. 652.
55. Bencini, A., Beni, A., Costantino, F., et al., *Dalton Trans.*, 2006, no. 5, p. 722.
56. Beni, A., Dei, A., Rizzitano, M., and Sorace, L., *Chem. Commun.*, 2007, no. 21, p. 2160.
57. Beni, A., Dei, A., Laschi, S., et al., C*hem.-Eur. J.*, 2008, vol. 14, no. 6, p. 1804.
58. Dei, A., Feis, A., Poneti, G., and Sorace, L., *Inorg. Chim. Acta*, 2008, vol. 361, p. 3842.
59. Dapporto, P., Dei, A., Poneti, G., and Sorace, L., C*hem.-Eur. J.*, 2008, vol. 14, no. 35, p. 10915.
60. Poneti, G., Mannini, M., Sorace, L., et al., *Chem. Phys. Chem.,* 2009, vol. 10, no. 12, p. 2090.
61. Dei, A., Poneti, G., and Sorace, L., *Inorg. Chem.*, 2010, vol. 49, no. 7, p. 3271.
62. Droghetti, A. and Sanvito, S., *Phys. Rev. Lett.*, 2011, vol. 107, no. 4, p. 47.
63. Patricia, T.T., Sandra, M.V., Manuela, L., et al., *Phys. Chem. Chem. Phys.*, 2012, vol. 14, no. 2, p. 1038.
64. Zhang, Y.-M., Li, A.-H., and Yu, F., *Acta Crystallogr., Sect. E: Struct. Rep. Online*, 2011, vol. 67, no. 7, p. m966.
65. Yu, F., *Acta Crystallogr., Sect. E: Struct. Rep. Online*, 2012, vol. 68, no. 10, p. m1248.
66. Bonnitcha, P.D., Kim, B.J., Hocking, R.K., et al., *Dalton Trans.*, 2012, vol. 41, no. 37, p. 11293.
67. Yu, F. and Li, B., *Inorg. Chim. Acta*, 2012, vol. 392, p. 199.
68. Panja, A., *RSC Adv.*, 2013, vol. 3, no. 15, p. 4954.
69. Jang, H.G., Cox, D.D., and Que, L., Jr., *J. Am. Chem. Soc.*, 1991, vol. 113, no. 24, p. 9200.
70. Chiou, Y.-M. and Que, L., Jr., *Inorg. Chem.*, 1995, vol. 34, no. 14, p. 3577.
71. Mialane, P., Tchertanov, L., Banse, F., et al., *Inorg. Chem.*, 2000, vol. 39, no. 12, p. 2440.
72. Jo, D.-H., Chiou, Y.-M., and Que, L., Jr., *Inorg. Chem.*, 2001, vol. 40, no. 13, p. 3181.
73. Pascaly, M., Duda, M., Schweppe, F., et al., *Dalton Trans.*, 2001, no. 6, p. 828.
74. Merkel, M., Pascaly, M., Wieting, M., et al., *Z. Anorg. Allg. Chem.*, 2003, vol. 629, nos. 12–13, p. 2216.
75. Merkel, M., Schnieders, D., Baldeau, S.M., and Krebs, B., *Eur. J. Inorg. Chem.,* 2004, no. 4, p. 783.
76. Merkel, M., Pascaly, M., Krebs, B., et al., *Inorg. Chem.*, 2005, vol. 44, no. 21, p. 7582.
77. Hitomi, Y., Yoshida, M., Higuchi, M., et al., *J. Inorg. Biochem.*, 2005, vol. 99, p. 755.
78. Higuchi, M., Hitomi, Y., Minami, H., et al., *Inorg. Chem.*, 2005, vol. 44, no. 24, p. 8810.
79. Simaan, A.J., Boillot, M.-L., Rivire, E., et al., *Angew. Chem., Int. Ed. Engl.*, 2000, vol. 39, no. 1, p. 196.
80. Floquet, S., Simaan, A.J., Riviere, E., et al., *Dalton Trans.*, 2005, no. 9, p. 1734.
81. Enachescu, C., Hauser, A., Girerd, J.J., and Boillot, M.L., *Chem. Phys. Chem.,* 2006, vol. 7, no. 5, p. 1127.
82. Girerd, J.-J., Boillot, M.-L., Blain, G., and Riviere, E., *Inorg. Chim. Acta*, 2008, vol. 361, nos. 14–15, p. 4012.
83. Harding, D.J., Harding, P., and Phonsri, W., *Coord. Chem. Rev.*, 2016, vol. 313, p. 38.
84. Collet, E., Boillot, M.-L., Hebert, J., et al., *Acta Crystallogr.*, 2009, vol. 65, no. 4, p. 474.
85. Kaszub, W., Buron-Le, CointeM., Lorenc, M., et al., *Eur. J. Inorg. Chem.,* 2013, nos. 5–6, p. 992.
86. Collet, E., Moisan, N., Balde, C., et al., *Phys. Chem. Chem. Phys.*, 2012, vol. 14, no. 8, p. 6192.
87. Tissot, A., Shepherd, H.J., Toupet, L., et al., *Eur. J. Inorg. Chem.,* 2013, nos. 5–6, p. 1001.
88. Mayilmurugan, R., Stoeckli-Evans, H., and Palaniandavar, M., *Inorg. Chem.*, 2008, vol. 47, no. 15, p. 6645.
89. Yu, F., Zhang, Y.-M., Li, A.-H., and Li, B., *Inorg. Chem.* Commun., 2015, vol. 51, p. 87.
90. Meer, M.V.D., Rechkemmer, Y., Breitgoff, F.D., et al., *Dalton Trans.*, 2016, vol. 45, no. 20, p. 8394.
91. Shultz, D.A., Bodnar, S.H., Vostrikova, K.E., and Kampf, J.W., *Inorg. Chem.*, 2000, vol. 39, no. 26, p. 6091.
92. Shultz, D.A., Vostrikova, K.E., Bodnar, S.H., et al., *J. Am. Chem. Soc.*, 2003, vol. 125, no. 6, p. 1607.
93. Shultz, D.A., Kumar, R.K., Bin-Salamon, S., and Kirk, M.L., *Polyhedron*, 2005, vol. 25, nos. 16–17, p. 2876.
94. Kirk, M.L., Shultz, D.A., Schmidt, R.D., et al., *J. Am. Chem. Soc.*, 2009, vol. 131, no. 51, p. 18304.
95. Kirk, M.L. and Shultz, D.A., *Coord. Chem. Rev.*, 2013, vol. 257, no. 1, p. 218.
96. Kirk, M.L., Shultz, D.A., Stasiw, D.E., et al., *J. Am. Chem. Soc.*, 2013, vol. 135, no. 45, p. 17144.
97. Tichnell, C.R., Shultz, D.A., Popescu, C.V., et al., *Inorg. Chem.*, 2015, vol. 54, no. 9, p. 4466.
98. Katayama, K., Hirotsu, M., Kinoshita, I., and Teki, Y., *Dalton Trans.*, 2014, vol. 43, no. 35, p. 13384.

99. Katayama, K., Hirotsu, M., Ito, A., and Teki, Y., *Dalton Trans.*, 2016, vol. 45, no. 25, p. 10165.

100. Frisch, M.J., Trucks, G.W., Schlegel, H.B., et al., *Gaussian-09. Revision E. 01*, Wallingford: Gaussian, 2013.

101. Tao, J.M., Perdew, J.P., Staroverov, V.N., and Scuseria, G.E., *Phys. Rev. Lett.*, 2003, vol. 91, no. 14, p. 146401.

102. Staroverov, V.N., Scuseria, G.E., Tao, J., and Perdew, J.P., *J. Chem. Phys.*, 2003, vol. 119, no. 23, p. 12129.

103. Bannwarth, A., Schmidt, S.O., Peters, G., et al., *Eur. J. Inorg. Chem.,* 2012, no. 16, p. 2776.

104. Cirera, J. and Paesani, F., *Inorg. Chem.*, 2012, vol. 51, no. 15, p. 8194.

105. Starikova, A.A. and Minkin, V.I., *Russ. J. Coord. Chem.*, 2018, vol. 44, no. 8, p. 483. https://doi.org/10.1134/S1070328418080079

106. Starikova, A.A., *Chem. Papers*, 2018, vol. 72, no. 4, p. 821.

107. Starikov, A.G., Starikova, A.A., Chegerev, M.G., and Minkin, V.I., *Russ. J. Coord. Chem.,* 2019, vol. 45, no. 2, p. 105. https://doi.org/10.1134/S1070328419020088

108. Cirera, J., Via-Nadal, M., and Ruiz, E., *Inorg. Chem.*, 2018, vol. 57, no. 22, p. 14097.

109. Starikov, A.G., Starikova, A.A., and Minkin, V.I., *Dokl. Chem.,* 2016, vol. 467, no. 1, p. 83.

110. Starikova, A.A., Chegerev, M.G., Starikov, A.G., and Minkin, V.I., *Comp. Theor. Chem.,* 2018, vol. 1124, p. 15.

111. Noodleman, L., *J. Chem. Phys.*, 1981, vol. 74, no. 10, p. 5737.

112. Shoji, M., Koizumi, K., Kitagawa, Y., et al., *Chem. Phys. Lett.*, 2006, vol. 432, nos. 1–3, p. 343.

113. Minkin, V.I., Starikov, A.G., and Starikova, A.A., *Pure Appl. Chem.*, 2018, vol. 90, no. 5, p. 811.

114. Bally, T., *Nature Chem.,* 2010, vol. 2, no. 3, p. 165.

115. Starikova, A.A., Metelitsa, E.A., and Starikov, A.G., *J. Struct. Chem.*, 2019, vol. 60, no. 8, p. 1219.

116. Starikov, A.G., Chegerev, M.G., Starikova, A.A., and Minkin, V.I., *Russ. J. Coord. Chem.,* 2019, vol. 45, no. 1, p. 675. https://doi.org/10.1134/S1070328419090082

117. Starikova, A.A. and Minkin, V.I., *Comp. Theor. Chem.,* 2018, vol. 1138, p. 163.

118. Rudebusch, G.E., Zafra, J.L., Jorner, K., et al., *Nat. Chem.,* 2016, vol. 8, no. 8, p. 753.

119. Nakano, M., Fukuda, K., and Champagne, B., *J. Phys. Chem. C*, 2016, vol. 120, no. 2, p. 1193.

120. Starikova, A.A., Metelitsa, E.A., and Minkin, V.I., *Russ. J. Coord. Chem.,* 2019, vol. 45, no. 6, p. 411. https://doi.org/10.1134/S1070328419060095

121. Minkin, V.I., Starikov, A.G., Starikova, A.A., et al., *Dalton Trans.*, 2018, vol. 47, no. 44, p. 15948.

Translated by E. Yablonskaya